MASARYKOVA UNIVERZITA
PŘÍRODOVĚDECKÁ FAKULTA
ÚSTAV TEORETICKÉ FYZIKY A ASTROFYZIKY

Bakalářská práce

BRNO 2018　　　　　　　　　　　　　　　**JIŘÍ ŽÁK**

MASARYKOVA UNIVERZITA
PŘÍRODOVĚDECKÁ FAKULTA
ÚSTAV TEORETICKÉ FYZIKY A ASTROFYZIKY

Analýza tvaru světelné křivky vybraných cefeid z Galaktického pole

Bakalářská práce

Jiří Žák

Vedoucí práce: Mgr. Marek Skarka, Ph.D.   **Brno 2018**

Bibliografický záznam

Bibliographic Entry

Abstrakt

Náplní této práce je získání originální *BVRI* CCD fotometrie 9 cefeid pulzujících v základním módu v souhvězdí Kasiopea. Pozorování probíhalo během podzimu 2017 a zimy 2018 na Observatoři Masarykovy Univerzity v Brně. Ze získaných dat byly sestrojeny fázové křivky pro každý filtr a následně popsány metodou Fourierovy dekompozice. Při porovnání získaných koeficientů Φ_{21}, Φ_{31}, R_{21} a R_{31} ve filtru *V* s daty z různých zdrojů v literatuře a s daty z projektu ASAS-SN nebyly zjištěny výrazné rozdíly. Byla provedena oprava pulzační periody pro V824 Cas. Tato hvězda vykazuje nezvykle nízkou amplitudu i Fourierovy amplitudové koeficienty, což by mohlo naznačovat vyšší metalicitu, jiný typ cefeid nebo dvojhvězdnost V824 Cas. Získané koeficienty byly také porovnány s koeficienty cefeid naměřenými projektem OGLE v *I* filtru v Galaktické výduti, LMC a SMC. Kromě V824 Cas a CF Cas žádná z hvězd nevykazovala výraznější odchylky od obecného trendu.

Abstract

This work presents original *BVRI* CCD photometry of 9 fundamental mode Cepheids in Cassiopeia constellation. Observation was carried out during autumn 2017 and winter 2018 at Masaryk University Observatory, Brno, Czech Republic. From obtained data, phase curves were constructed for each filter. Light curves were described using Fourier decomposition technique. The comparison of obtained coefficients Φ_{21}, Φ_{31}, R_{21} and R_{31} in the *V* filter with the coefficients from various sources in the literature and with the data from the ASAS-SN project did not show any major discrepancy. An estimation of a new pulsation period was done for V824 Cas. This Cepheid exhibits unusually low amplitude and amplitude Fourier coefficients. This may be explained by higher metallicity, by being a different type of Cepheid or by a presence of an unseen binary companion. The acquired coefficients in the *I* filter were additionally compared to the coefficients obtained by the OGLE project for the Galactic Bulge, LMC and SMC Cepheids. With exception of V824 Cas and CF Cas, no other star shows any major deviation from general trends.

MASARYKOVA UNIVERZITA
Přírodovědecká fakulta

ZADÁNÍ BAKALÁŘSKÉ PRÁCE

Akademický rok: 2017/2018

Ústav: Ústav teoretické fyziky a astrofyziky

Student: Jiří Žák

Program: Fyzika

Obor: Fyzika

Ředitel *Ústavu teoretické fyziky a astrofyziky* PřF MU Vám ve smyslu Studijního a zkušebního řádu MU určuje bakalářskou práci s názvem:

Název práce: Analýza tvaru světelné křivky vybraných cefeid z Galaktického pole

Název práce anglicky: Light-curve diagnostics of selected Galactic field classical Cepheids

Oficiální zadání:
Classical delta Cepheid type stars play crucial role in modern astrophysics, mainly in mapping the universe. The aim of the project is to get original multicolour photometry of selected Cepheids at Masaryk University Observatory and/or at other observatories, calibrate the data to standard Johnson-Cousins photometric system, and describe the light-curve shape using standard Fourier decomposition techniques. The student will discuss the shape of the light curves in all passbands and compare them with the light-curve parameters of Cepheids observed by the OGLE survey and Cepheids from the Galactic field.

Literatura:
AERTS, Conny, Jorgen CHRISTENSEN-DALSGAARD a Donald, W. KURTZ. *Asteroseismology*. 2010. ISBN 978-1-4020-5803-5.

CATELAN, Marcio a Horace, A. SMITH. *Pulsating stars*. 2015. ISBN 978-3-527-40715-6.

Jazyk závěrečné práce: angličtina

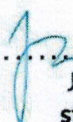**Vedoucí práce:** Mgr. Marek Skarka, Ph.D.

Konzultant: doc. RNDr. Miloslav Zejda, Ph.D.

Datum zadání práce: 26. 10. 2017

V Brně dne: 28. 11. 2017

Souhlasím se zadáním (podpis, datum): 4. 1. 18

....
Jiří Žák
student

....
Mgr. Marek Skarka, Ph.D.
vedoucí práce
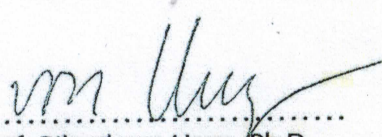
....
prof. Rikard von Unge, Ph.D.
ředitel Ústavu teoretické fyziky a astrofyziky

Acknowledgement

Declaration of originality

I hereby declare that this thesis represents my original work and that I have used no other sources except as noted by citations.

Brno, May 22 2018

_____
Jiří Žák

Contents

Introduction

Cepheids have played a prominent role in the history of astronomy. It was these stars that allowed mankind to truly understand how spacious the universe actually is. Cepheids were among the first variable stars discovered at the end of the 18th century. It was later discovered that they change their brightness due to stellar pulsations. H. Leavitt discovered the famous Period-Luminosity (P-L) relation in 1912, which ties the absolute magnitude and pulsation period. This allowed unprecedented distance measurements.

Cepheids are characterized by their light curve. The shape of the light curves changes with the pulsation period. The amplitude of the light variations is also period dependent, since it increases towards longer periods. In addition, the amplitude increases towards shorter wavelengths. All these characteristics reflect the physical conditions of Cepheids and can tell us something about these important stars. In spite of observing Cepheids over 100 years, they are still frequent targets. Cepheids are extremely useful when testing recent hydrodynamical models.

The objective of this thesis is to obtain original *BVRI* photometric data of selected fundamental more Cepheids in the Cassiopeia constellation, their subsequent analysis and description of their light curves using Fourier decomposition technique. The thesis is divided into five chapters. A brief presentation of Cepheids as variable stars, their types, evolution and physical processes behind pulsations are given in the first chapter. The second chapter deals with used methodology. The principles of CCD photometry are given, terms connected to light curves, such as epoch and phase, are introduced. Further on, the Fourier decomposition technique is described in details. Obtaining original data is thoroughly discussed in the third chapter. In the fourth chapter, obtained results are described. Light curve and Fourier coefficients for each of the selected Cepheids are presented and discussed.

Chapter 1

Cepheids

1.1 Cepheids as variable stars

History of Cepheids observations spans a long period of time. It was Edward Piggot in 1784 who noticed that η Aquilae is a variable star and John Goodrick who made this discovery for eponymous star δ Cephei. However, the origin of its variability remained unexplained for many decades. After many unsuccessful attempts to explain the light curve variability of Cepheids due to various reasons such as starspots or eclipses (Catelan & Smith, 2015), it was unveiled that the variability originates from stellar pulsations.

Schwarzschild (1900) discovered that the amplitude of a Cepheid's luminosity variation is greatly higher in photographic light than in visual light. Such phenomena pointed to a variability of the temperature as well as of the luminosity. These facts found their natural explanation in the hypothesis of Cepheid pulsation. This idea was originally proposed by Ritter (1879) and later by Plummer (1914) and Shapley (1914). However, they did not explain the mechanism of the pulsations. It was Eddington (1917) who unveiled the mechanism of pulsations. His idea was that pulsation might occur in stars if the stars behave as thermodynamic engines.

At the same time, Cepheids and many other stars were being observed under the leadership of Edward Pickering at Harvard Observatory. One of his assistants, Henrietta Leavitt, noticed a relationship between period and luminosity for certain stars in the Magellanic Clouds after examination of hundreds of photographic plates. She discovered that Cepheids obey a P-L relation (Leavitt & Pickering, 1912). Hertzsprung (1913) realized that if P-L relation could be calibrated, then the absolute magnitudes could be determined directly from their periods.

1.2   Types and evolution

1.2.1   Types

Cepheids are variable stars that can be divided into two basic categories. Classical Cepheids (Type I) or Type II. The former are young stars (population I stars). Type II Cepheids are old stars (population II), they are less luminous at given period and less massive than the Type I (Catelan & Smith, 2015). Both types follow distinct P-L relation. Only classical Cepheids will be discussed in this thesis, so the adjective "classical" will be omitted further on.

Typical Cepheid is a young star with intermediate mass which is a white-yellow population I supergiant. Cepheids are radial pulsators which show periodic variations in radii, temperature, and brightness. The pulsation periods of Cepheids range from around 1 day to as long as 60 days but there are Cepheids observed in the Magellanic cloud whose period is over 100 days (Ulaczyk, Szymański, Udalski, et al., 2013).

Mass	3.5 to 15$M_\odot$
Luminosity	300 to 25000 $L_\odot$
Radius	15 to 200 $R_\odot$
Spectral Type	F-K giant and supergiant
T_{eff}	6000 to 8000 K
Pulsation period	1 to 100 days
Absolute V mag.	-0.5 to -6 mag
V-band variability	0.5 to 1 mag
Age	10^7 to 10^8 years

Table 1.1: Typical properties of classical Cepheids. Data from Cox (1980) and Percy (2007).

1.2.2   Evolution

Cepheids are evolved stars which have already left the main sequence. Since they are intermediate stars they were able to ignite He combustion under non-degenerate conditions. However, after they have exhausted He in their core they developed electron degenerate carbon-oxygen core. To become a Cepheid, it is necessary for the star to be in a post core hydrogen burning phase as well as to pass through the instability strip. The instability strip is a narrow almost vertical region in the Hertzsprung-Russel (HR) diagram[1] where the classical pulsating variable stars are located. Cepheids temperature ranges between 6000 K to 8000 K (Percy, 2007).

---

[1]HR diagram is a plot of stars showing dependency between star's absolute magnitude or luminosity versus their spectral classification or effective temperature.

During their lifetime, Cepheids may cross the instability strip on the HR diagram several times. The first crossing of the instability strip occurs while the hydrogen-shell burning phase is happening and the star is evolving to cooler temperatures to become a red giant. Time needed for the first crossing is relatively short, it corresponds to the Kelvin Helmholtz timescale which ranges from 10^3 to 10^4 years (Fadeyev, 2014). Due to the shortness of this crossing, only a few percents of known Cepheids are expected to be in this phase. In less massive stars, the second crossing of the instability strip occurs once the star has ignited He in its core. The stars start to evolve to higher temperatures, however, this process is reversed after some time and the star may loop through the instability strip. This is called a blue loop and produces the second and the third crossing of the instability strip. The timescale of these loops can be several million years (Fadeyev, 2014).

1.3   Origin of Cepheid pulsations

1.3.1   Radial Pulsations

A star is a gravitationally bound object in a state of hydrostatic equilibrium. Every point of a star is precisely balanced by gravitation force and by the pressure gradient. In this case, equilibrium is stable which means that if the star is perturbed and the equilibrium is disrupted, the force that is trying to return the system into equilibrium is increased. During the return to the equilibrium, the force does not diminish immediately, it continues to act until opposite force starts to counteract. Movement stops and changes direction. If this is happening to the star as a whole, we call this radial pulsations. It can be shown that for small amplitudes the period of the action is independent of its amplitude and is equal to the natural period of oscillations of the star.

Certain conditions must be met in order for a pulsation to occur and hold. The overall work done by the system during pulsation cycle must be positive. According to the 1st and the 2nd law of thermodynamics we can write

$$W = \oint \frac{\delta Q(t)\, \delta T(t)}{T_0} > 0, \tag{1.1}$$

where T_0 is always positive. For the equation above to be true, δQ and δT must both be either positive or negative. This implies that with increasing temperature the heat is increasing as well. On the other hand, when the temperature is decreasing the heat is being released.

There can be found many ways to derive the basic pulsation period in the literature, the following one is taken from Mikulášek & Zejda (2013).

According to the virial theorem in a gravitationally bound object, the absolute value of potential energy is equal twice the kinetic energy

$$2 \langle E_k \rangle + \langle E_p \rangle = 0, \tag{1.2}$$

where E_k is the kinetic energy and E_p is the potential energy.

The matter inside a star can be thought as an ensemble of chaotically moving particles hence we can write their kinetic energy as

$$E_k = \frac{1}{2} M v_s^2. \tag{1.3}$$

We can express potential energy as

$$E_p \sim \alpha \, G \, \frac{M^2}{R} = 2 \, E_k = M \, v_s^2, \tag{1.4}$$

where α is a star mass distribution coefficient (usually equal to 1.6), G is the gravitational constant, M is the mass of the star and R is the radius of the star. Mean velocity of the particle is then defined as

$$v_s^2 = \alpha \, G \, \frac{M}{R}. \tag{1.5}$$

The mean velocity of the particles in the star is roughly equal to the speed of sound. We can define a fundamental period of radial pulsation Π as a time that is necessary to carry information about pressure change across the diameter of the star. This time is equal to $\frac{2R}{v_s}$ and, thus, for the basic pulsation period we can write

$$\Pi \approx \frac{2 \, R}{v_s} = \sqrt{\frac{4 \, R^3}{\alpha \, G \, M}} \cong \frac{1}{\sqrt{G \, \bar{\rho}}}. \tag{1.6}$$

Period of natural oscillation of the star is thus stellar mean density function. This is in a good agreement with the observations, as stars with low densities as Mirids pulsate with a period of hundreds of days, while denser Cepheids pulsate within order of tens of days and stars of delta Scuti type pulsate with periods in the order of a few hours or less.

An amplitude of the pulsations is a function of stellar radius. A node of the pulsation always lies in the center of a star. Fundamental mode Cepheids pulsate in one direction only, the whole star is either expanding or collapsing. For overtone Cepheids apply that additional nodal sphere is located between the center and the surface of the star. The matter between nodes is then moving in opposite directions. Most of known Cepheids pulsate in the fundamental mode. Other Cepheids pulsate in first overtone, second overtone or even higher modes of pulsation. There are known cases of Cepheids that pulsate in more than one mode simultaneously (Soszyński, Udalski, Szymański, et al., 2017).

1.3.2 Pulsation mechanisms

Observation of large sample of variable pulsating stars has shown that some stars' amplitude of the pulsation does not show any secular changes. This means that the pulsations are always donated by new energy and are stable over decades. There is a need for a mechanism that compensates losses due to the friction in the interior of every pulsating star. If there is not a one, pulsations would dampen and the star would be in a state of hydrostatic equilibrium.

Radial pulsations use radiant flux as a source of energy. In order for pulsations to be sustained, there need to be regions of the star that are able to absorb required energy during stellar compression and release accumulated energy during its expansion. However, this condition is rarely met. Usually stellar matter obeys Kramer Opacity law $\kappa \propto \rho \, T^{-3.5}$. If the matter is adiabatically compressed, density and temperature increases but opacity decreases, so the matter is less optically thick and the energy is not trapped. This behavior does not allow pulsation to arise.

It was Eddington (1926) who proposed a valve mechanism. According to him, a certain layer of matter should exist inside a star, that its opacity would increase during compression. This layer should be able to absorb enough energy to block the flow from the core and during the forthcoming expansion release it. Eddington stated that the supply of energy is not an issue. The question was what is the mechanism that is responsible for transferring this energy into a mechanical work. Pulsating stars work similarly to thermodynamic engines with heat being added to matter at a high temperature only to be withdrawn at a low temperature.

Zhevakin (1953) has developed Eddington's ideas further and calculated precise conditions for pulsations. Another significant contribution was done by Cox (1980) who confirmed that the valve mechanism as proposed by Eddington can work in regions with the partially ionized matter.

The adiabatic theory implies that there might be three mechanisms involved. An ϵ mechanism which is responsible for energy generation. The κ and γ mechanisms are involved in energy transfer. The κ mechanism is the most significant in Cepheids (Catelan & Smith, 2015). For this reason, only the κ mechanism will be discussed further.

The κ mechanism is based on the phenomena that during stellar contraction, part of the energy within the active layer is used for element ionization and thus relative opacity increases. Opacity increase causes gas and radiation pressure increment which is strong enough to uplift the layer. The layer is expanding as it moves upwards where is lower density and temperature. This leads to rapid atom recombination and energy release. However, the layer is not cooling sufficiently quickly with respect to the surroundings. In addition to layer density decrease, this leads to relative opacity decrease. The weight of the upper layers causes that the layer starts to move downwards and the whole cycle repeats.

In most stars, there are two active driving mechanism layers. First one is a broad layer that contains ionized hydrogen as well as once ionized helium. This layer is located in depths with a temperature between 10 000 to 15 000 K (Glazebrook, 2010).

However, this layer is significant only in a small fraction of pulsating stars. It is most probably essential to pulsations in Mirids. A layer of partially ionized helium with a temperature around 40 000 K is important for the most of radially pulsating stars (Glazebrook, 2010). This layer roughly contains an equal representation of once ionized helium He II and twice ionized helium He III. However, for pulsations to be sustainable, this layer must be located within certain depth. In case of stars with low effective temperature, the layer would be too deep, that a convection and a substantial friction would hinder the pulsation mechanism. In case of very hot stars, the layer is located too close to the surface where the layers are relatively thin and of a low mass. Low-mass active layers are not sufficient to retain enough energy to supply heat losses during pulsation, this implies the existence of the instability strip.

1.3.3   Hertzsprung Progression

Hertzsprung (1926) made a discovery that certain Cepheids show a relationship between the position of a bump on the light curve and the pulsation period. This phenomenon was named the "Hertzsprung progression". Ledoux & Walraven (1958) found a similar bump in radial velocity curves.

   Empirically it was found that Cepheids with pulsation period in a range $6 < P < 16$ d show a bump along the light and the velocity curves. This feature appears on the descending branch of the light curve for Cepheids whose pulsation period is shorter than 9 days. It is positioned around the maximum of the light curve for Cepheids with pulsation period between 9 and 12 days and moves to the ascending branch for Cepheids with longer periods.

   This feature is still not satisfyingly explained. There are two distinct models that attempt to explain the appearance of the bump. Whitney (1956) proposed the *echo* model. According to his model, the bump is caused by a pressure excess in the first He ionization region that generates pressure waves moving inward and outward. As the former reaches the stellar core close to the phase of maximum radius, then reflects and reaches the surface one cycle later causing the appearance of the bump. The *resonance* model was proposed by Simon & Schmidt (1976). Their work tries to explain the bump as a resonance between the second overtone and the fundamental mode and it takes place when the period ratio between these two modes is close to 0.5.

1.4   Period-Luminosity relation

A relation between period and magnitude of Cepheids was firstly noticed by Henrietta Swan Leavitt (Leavitt & Pickering, 1912). She was working on data analysis of a systematic survey of the Magellanic clouds. She has determined a period of several Cepheids and noticed that the brighter ones have longer periods. Stars in each of the Magellanic clouds are approximately of the same distance from us. This suggested that the absolute magnitudes are a function of a period. Leavitt & Pickering (1912) published graphs

(Figure 1.1), where period and logarithm of a period were plotted against magnitude. The later graph has shown clear linear dependency. However, this dependency could not be calibrated due to the constraint that no Cepheid had measured parallax at that time.
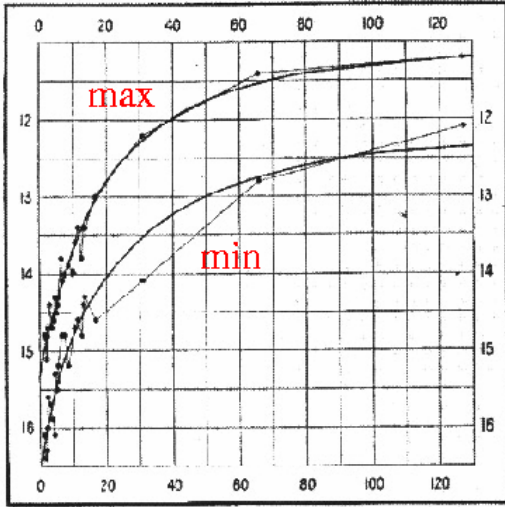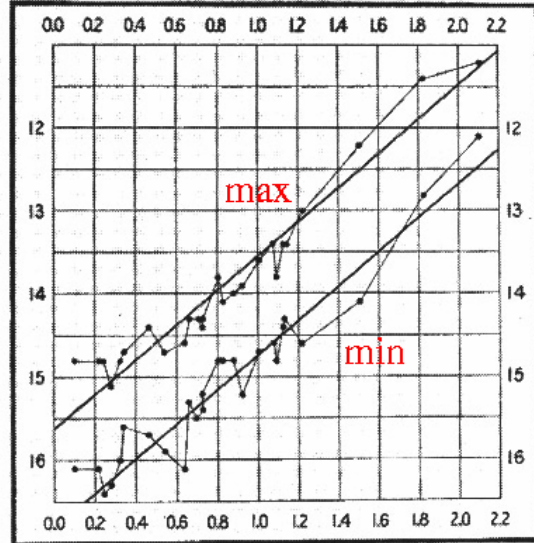

Figure 1.1: Magnitude to period dependence (left) and magnitude to logarithm of the period dependence (right) (Leavitt & Pickering, 1912).

It was Hertzsprung (1913) who observed several Cepheids and measured their distances. He subsequently published the following relation

$$M_V = -0.6 - 2.1 \log \Pi. \tag{1.7}$$

His work suffered from two major flaws. He did not account for interstellar extinction. In addition, he did not distinguish between two distinct populations of Cepheids which have different P-L relation. He calculated the distance of Small Magellanic cloud as 900 pc. Kukarkin (1949) showed that RR Lyrae stars follow different P-L relation. This allowed for much precise calibration of the P-L relation.

A complex work by Madore & Freedman (1991) gives P-L relations in several filters from many observations of Cepheids in LMC. They published following relation for magnitude in *V* filter

$$M_V = -2.88(\pm 0.20) \log \left(\frac{\Pi}{10\,\mathrm{d}} \right) - 4.12(\pm 0.09)[\pm 0.29], \tag{1.8}$$

where the uncertainty given in square brackets is the scatter around the mean relation.

One of the most recent determination of the P-L relation was obtained using the Hubble Space Telescope (Benedict, McArthur, Feast, et al., 2007). Absolute trigonometric parallaxes measurements of nine galactic cepheids were obtained to get the following calibration of the P-L relation

$$M_V = 2.43\,(\pm 0.12)\,(\log \Pi - 1) - 4.05\,(\pm 0.02)\,. \tag{1.9}$$

1.4.1 Explanation of the P-L relation

Cepheids and many other pulsators are located in the instability strip of the HR diagram. Therefore the effective temperatures of these stars are closely similar and only weakly dependent on luminosity. Luminosity is defined as $L = 4\pi R^2 \sigma T_{\text{eff}}^4$ with $T_{\text{eff}} \sim$ constant, thus, for Cepheids, $L \propto R^2$. As shown in subsection 1.3.1 the pulsation period of the fundamental mode is given as

$$\Pi \sim (G\,\bar{\rho})^{-1/2} \propto \left(\frac{M}{R^3}\right)^{-1/2}, \tag{1.10}$$

We can eliminate the stellar radius R in favor of M and L to write

$$\Pi \propto L^{3/4}\,M^{-1/2}. \tag{1.11}$$

Since L is usually a sensitive function of mass, equation 1.11 implies a relation $\Pi \propto L^x$ with $x \leq 3/4$ since $dM/dL > 0$. However our intial assumption is not completely valid as T_{eff} is not strictly a constant within the instability strip. Temperature slowly decreases as L increases. The empirical relation 1.8 indicates $\Pi \propto L^{0.87 \pm 0.06}$ if the variations in the bolometric correction are ignored (Knapp, 2011).

Chapter 2

Methodology

2.1 Photometry

The main task of stellar photometry is to measure stellar brightness. Historically, photometry was carried out using photoelectric photometer which is a device that measures star's brightness by producing an electric current when light falls on a light-sensitive surface using photoelectric effect. In last decades they were replaced by much cheaper and easily accessible charged coupled device (CCD). However, they are still used when a high-speed photometry is used as photomultiplier can work on time scales shorter than a millisecond (Santhanam & Bhattacharyya, 1985).

2.1.1 CCD photometry

For many years, amateur astronomers were doing mostly visual photometry. It has changed with the invention of the CCD camera and their widespread usage. Nowadays, CCD cameras are widely used by both amateur and professional astronomers for photometry. First CCD was introduced in 1969 at the Bell Laboratories in the USA (Boyle & Smith, 1970). A CCD camera which was introduced year later is an integrated circuit etched onto a silicon surface forming light-sensitive elements called pixels. Photons that hit the silicon surface and produce free electrons through the photoelectric effect. After being released, electrons do not fly away, they are trapped at place by a potential well. These electrons are subsequently read by electronics.

Exposure time is defined as the length of time when the sensor inside of the CCD camera is exposed to light. A dynamical range of CCD cameras is given by the ADC converter. There is a range of 65 535 ADU for the 16-bit converter. A case when a pixel has too many electrons in it and electrons start to spill around the afflicted pixel is called blooming. There are methods how to prevent blooming from happening by introducing anti-blooming structures. However, these structures can reduce the effective quantum efficiency or introduce nonlinearity into the sensor. Thus, it is not recommended to use anti-blooming structures for high-precision measurements.

Differential photometry is a process of a measuring brightness of a star relative to a control (standard) star that has a constant luminosity. Although we are unable to find out the brightness of the star directly in a standard system, it is very helpful to study how the star's brightness changes over time.

2.1.2   Correction frames

After reading out the CCD chip, raw data are obtained. These data are not suitable for further analysis without applying correction frames. Raw data suffer from many deviations.

One of the most prominent is the dark current. During long exposures even with moderate cooling, a significant amount of electrons can be produced in the CCD pixel due to thermal excitation. Thermal energy is sufficient to excite some electrons which are unrecognizable from image electrons and contribute to the noise. A general rule is that for every 7-8° C of cooling, there is about twice the reduction in the dark current (Postec, 2012). Some pixels may have extraordinarily high dark current, these are called hot pixels. Elimination of dark current is done by obtaining series of dark frames which are frames with closed shutter with the same exposure time as a data frame. After combining several such frames, a median frame called masterdark is obtained. Subtraction of masterdark from obtained data frames is done by a software in subsequent analysis.

Flat field frame is a correction frame that accounts for distinct pixel sensibility on the CCD chip, inequality of illuminating the CCD chip as well as any dust and dirt in the path of light in the optical system. Procedure for obtaining flat field frame is to acquire series of several frames in each filter and combine them to obtain frame called masterflat. Cloudless sky after sunset can be used for obtaining flat field frames. Each flat field frame must be corrected for a dark frame. After performing dark current corrections, the data frame is divided by the flat field frame to obtain calibrated data frame ready to use for science research.

2.2   Filters

In modern astronomy, sets of well-defined filters are widely used to acquire astronomical data. Photometric systems were introduced to investigate radiation on selected wavelengths. Furthermore, it allowed better data comparison between different observers and observatories. Filters allow the light to pass only in the selected range of electromagnetic spectrum.

Filters are usually divided into three categories according to the width of their passbands. There are broadband systems which have passbands wider than 30 nm. Then Intermediate systems exist with passband width between 30 and 10 nm. At last, we have narrowband systems with passband width less than 10 nm wide.

One of the most widely used systems is the one defined by Johnson & Morgan (1953). It consists of 3 filters. Filter *U* allows light of wavelengths between 300 nm and 420 nm

to pass through. Filter *B* has transmissivity between 360 and 420 nm and *V* filter has transmissivity between 460 and 740 nm.

Johnson and his coworkers used 1P21 photomultiplier to measure many thousands of stars and have published their *UBV* magnitudes. This allowed the general usage of (*U-B*) and (*B-V*) color indices which characterize effective temperatures of the stars.

This system was subsequently enlarged to consist of more filters in the red and infrared regions: broadband filters *R* (700 nm), *I* (900 nm), *J* (1250 nm), *K* (2200 nm) and *L* (3400 nm) (Bessell, 2005). One of the disadvantages of this system is that the short wavelength cutoff of the *U* filter is set mostly by the Earth's atmosphere rather than the filter itself. This can cause that the observation can be altitude dependent. Another disadvantage of the system is that the *U* and *B* filter do overlap each other and thus the height of the Balmer jump cannot be determined.
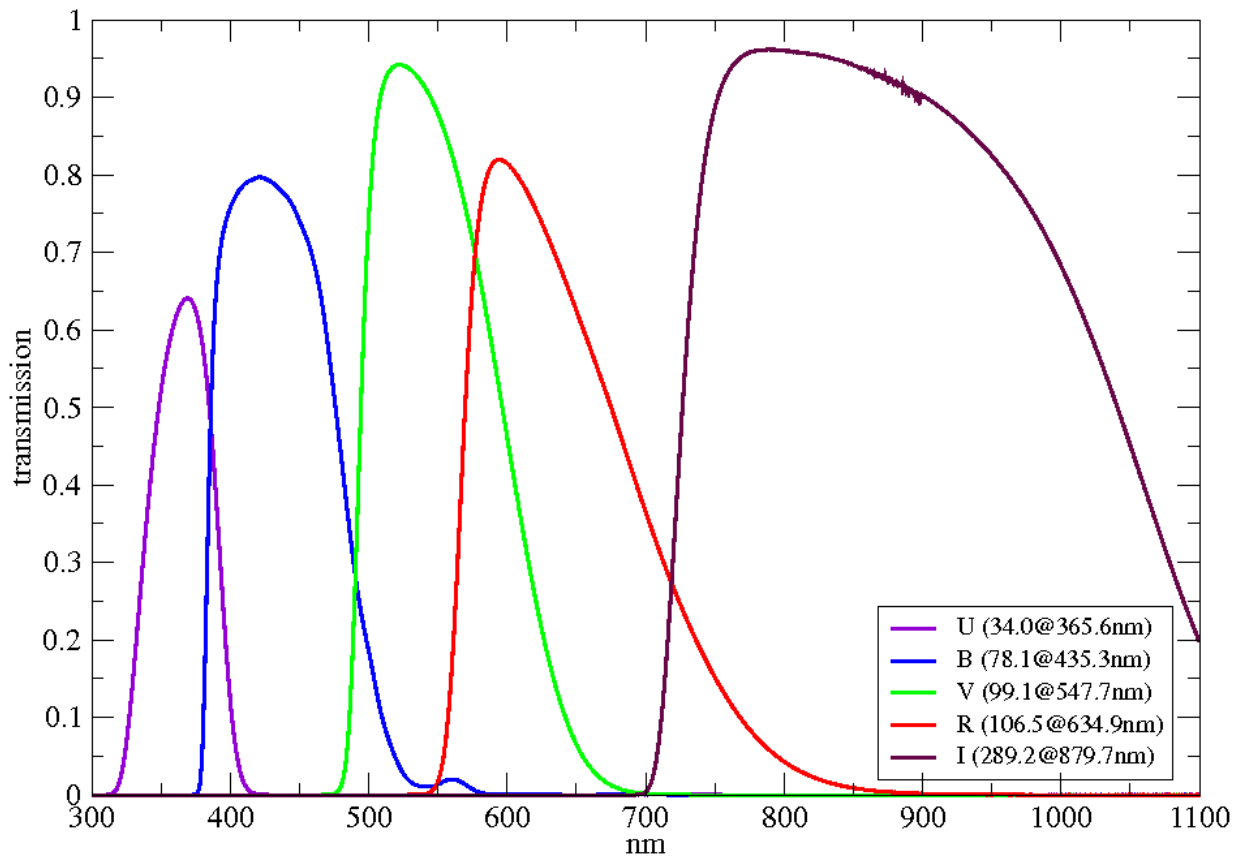

Figure 2.1: *UBVRI* photometric system (Bessell, 2005).

2.3   Light curve, epoch, phase, phase function

2.3.1   Light curve

A light curve is a graph of the changes in brightness of a star over time. Brightness is usually expressed in magnitudes and time in Julian date. We distinguish periodic and aperiodic light curves. Light curves of periodically variable stars have many advantages. The most important one is that the shape of such periodic light curves stays identical for many cycles. However, periodic light curves can show secular changes. The shape of the light curve or the period is changing in this case. To make things more interesting, there can be multiple secular changes superimposed onto each other. Examples of periodic light curves are light curves of Cepheids and other periodically pulsating stars, transiting exoplanets and eclipsing binaries. Aperiodic light curves have supernovas, novas, and cataclysmic stars.

Light curves are useful in many ways. Amplitude and period of pulsation reflect physical characteristics of the stars. Also, the shape of the light curve can tell us something about the pulsation mode. Periodic events are very useful. For example, the time separation of maximum light of asteroid light curve can give an estimate of its rotational period.
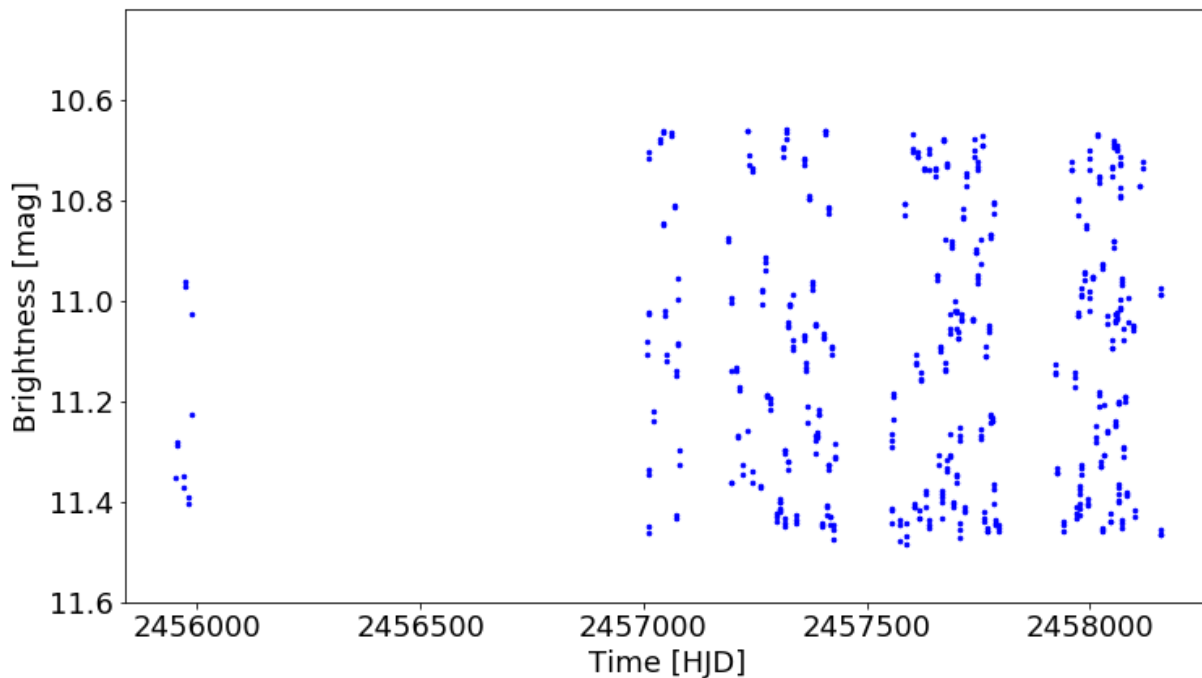

Figure 2.2: Example of a light curve (ASAS-SN).

2.3.2 Epoch

The actual state of a periodically changing variable star is usually described with two time-dependent functions. The first one is called an epoch $E(t)$ and is defined as

$$E(t) = \text{floor}[\frac{t - M_0}{P}],\tag{2.1}$$

where t is time, M_0 is the phasing moment and P is the period. It is a nondecreasing step function which represents the number of cycles that has passed since M_0, which is usually time of light extremum (minimum or maximum) in the past.

2.3.3 Phase

Phase $\Phi(t)$ is the second function and is defined as

$$\Phi(t) = \text{frac}[\frac{t - M_0}{P}].\tag{2.2}$$

It is a triangle wave function that is minimal at the beginning of a new cycle $\Phi = 0$ and then monotonically grows to reach the value of maxima at the end of the cycle when $\Phi = 1$. Phase is particularly useful for shape and shape stability investigation of curves of various quantities.

2.3.4 Phase function

Another way how to describe a state of a periodically changing star is to use a phase function $\theta(t)$ that is defined as follows

$$\theta(t) = E(t) + \Phi(t).\tag{2.3}$$

Phase function of a variable star $\theta(t)$ is a monotically growing smooth time dependent function that passes through origin at the beginning of time epoch $t = M_0$; $\theta(M_0) = 0$.

2.4 Fourier decomposition of the light curve

Due to the periodic nature of Cepheid light curves, the data points from well-observed Cepheids can be described using the technique of Fourier decomposition. This technique was introduced by Schaltenbrand & Tamman (1971). Further studies have been discussed and developed by Simon & Lee (1981) to study structural properties of Cepheid light curves.

It was assumed that each light curve is sctrictly periodic and can be represented by Fourier series:

$$m(t) = A_0 + \sum_{i=1}^{N} a_i \, \cos(i\omega(t - t_0)) + \sum_{i=1}^{N} b_i \, \sin(i\omega(t - t_0)), \tag{2.4}$$

where *m(t)* is the observed magnitude at time t, A_0 is the mean magnitude, a_i, b_i are the amplitude components of (i-1)th harmonic, $\omega = 2\pi/P$ is the angular frequency, P is the period in days, N is the order of the series and t_0 is an arbitrary moment in the past (usually a maximum or a minimum light is used).

The previous equation has $2N + 1$ unknown parameters which require at least the same number of data points to solve for these parameters. Equation 2.4 can be rewritten as

$$m(t) = A_0 + \sum_{i=1}^{N} A_i \, \cos(i\omega(t - t_0) + \phi_i), \tag{2.5}$$

where $A_i = \sqrt{a_i^2 + b_i^2}$ and $\tan \Phi_i = -\frac{b_i}{a_i}$.

A CEPHEUS program written by Barnacka (2014) is designed for operations with the data, light and phase curves. It also allows for Fourier series fitting, which is defined in CEPHEUS as

$$m(x) = A_0 + \sum_{k=1}^{N} A_k \, \sin(2\pi kx + \phi_k), \tag{2.6}$$

where $x = \frac{(t-t_0)}{P}$.

Phase independent Fourier parameters are defined as

$$R_{i1} = \frac{A_i}{A_1}; \phi_{i1} = \phi_i - i\phi_1, \tag{2.7}$$

where i is greater than 1. Transformation relations between sine series and cosine series are defined as

$$\Phi_{21}^{s} = \Phi_{21}^{c} - \frac{\pi}{2}, \tag{2.8}$$

$$\Phi_{31}^{s} = \Phi_{31}^{c} - \pi. \tag{2.9}$$

Coefficients R_{i1} and Φ_{i1} can be used to describe the shape of the light curve. These coefficients can be extremely useful when comparing real light curves between each other and with those resulting from hydrodynamic modeling. In addition, they can be of a great benefit when distinguishing various types of periodical stellar variability.

2.5   Transformation to a standard photometric system

Since each CCD, filter and telescope has different color response, data are often obtained by different observers, at different locations and time, it is important to standardize the data before putting them together. To be able to transform the obtained differential magnitudes of observed stars, we need to know the color of the stars and the effect of that color on the differential magnitude we obtained. The used methodology considers a linear relationship.

As a result of performing differential CCD photometry which compares the brightness of the variable star to the comparison star that lies in the same field of view, one is able to neglect atmospheric extinction because the air mass is for both stars almost the same. It is also prudent to select control star with the same color indices to be able to neglect color extinction.

The following transformations are used to perform calibration into the standard Johnson-Cousins system:

$$
\begin{aligned}
\Delta B - \Delta v &= C_B \cdot (\Delta b - \Delta v) + k_1, \\
\Delta V - \Delta v &= C_V \cdot (\Delta v - \Delta r) + k_2, \\
\Delta R - \Delta v &= C_R \cdot (\Delta v - \Delta r) + k_3, \\
\Delta I - \Delta v &= C_I \cdot (\Delta v - \Delta i) + k_4.
\end{aligned}
\tag{2.10}
$$

Capital letters denote differential magnitude in a standard system. Small letters denote differential magnitude in an instrumental system. For a color calibration, we can use so-called standard fields containing stars with wide variety of colors that were observed, for example, by Landolt (1983), Henden (1999) and others.

After observing standard fields, differential photometry is performed. Instrumental differences of magnitudes are obtained for each filter. The least square method is used to obtain calibration coefficients C_B, C_V, C_R and C_I.

Chapter 3

Observation

3.1 Choosing variable stars

At the beginning of this project, a search for optimal stars that would be suitable for our study has been conducted. It has been decided to obtain multicolor photometry only of fundamental mode Cepheids omitting overtone Cepheids. Since observation would have been carried out from late September to early March, there was a need to find a suitable part of the sky which allows observation during this period. Cassiopeia constellation was identified as a good area for our needs. Dense stellar fields of the Milky Way Belt that contains Cepheids are located in this constellation. Many of them were already well observed before, however, some of them required additional observation.

It has been decided to observe Cepheid with similar brightness to allow for similar exposure times. Similiar exposure times reduced the number of dark frames needed to be obtained each night. The sample of Cepheids was chosen to accommodate Masaryk University Observatory (MUO) telescope's characteristics. VSX catalog[1] (Watson, Henden, & Price, 2006) was used to eliminate Cepheids that were brighter than 10.3 magnitude in their maxima in *V* filter to ensure that the star would not saturate with exposure over 10 seconds. On the other hand, we omitted stars fainter than 11.8 magnitude in their minima in *V* filter to avoid exposures over 90 s in *B* filter and to ensure good signal to noise ratio. Another criterium was that the variable star was not in proximity to other stars for at least 10" as this would make obtaining precise light curves difficult with various seeing and weather conditions. ALADIN software (Bonnarel, Fernique, Bienaymé, et al., 2000) was used to obtain magnitude and other information.

After performing these steps, 9 Cepheids in 8 star fields that have matched our criteria has been selected. List of the stars with brief information is provided in the Table 3.1.

From Figure 3.1 we can see that the sample covers almost 1 magnitude in the (*B-V*) index, however, we can see in Table 3.1 that all selected stars are of a similar spectral type. It shows that the interstellar extinction changes significantly with the position on

---

[1]https://www.aavso.org/vsx/

the sky. CH Cas, which has the largest *(B-V)* index, has also the longest period, thus, it lies further and is affected the most by the interstellar extinction.

Star name	Period [days]	Sp. type	*V* [mag]	*(B-V)* [mag]
DF Cas	3.832472	F6-G4	10.53 - 11.13	1.372
V395 Cas	4.037728	G3	10.39 - 10.95	0.827
UZ Cas	4.259459	F6-G2	10.93 - 11.73	1.082
CG Cas	4.36554	F5-F8	10.89 - 11.73	1.228
CF Cas	4.87522	F8Ib-G0Ib	10.80 - 11.47	1.156
DW Cas	4.99776	F7	10.81 - 11.41	1.288
V824 Cas	5.359		11.03 - 11.36	1.272
BP Cas	6.272724	F6-G1	10.55 - 11.33	1.537
CH Cas	15.09215	F3pIb-F6	10.47 - 11.56	1.755

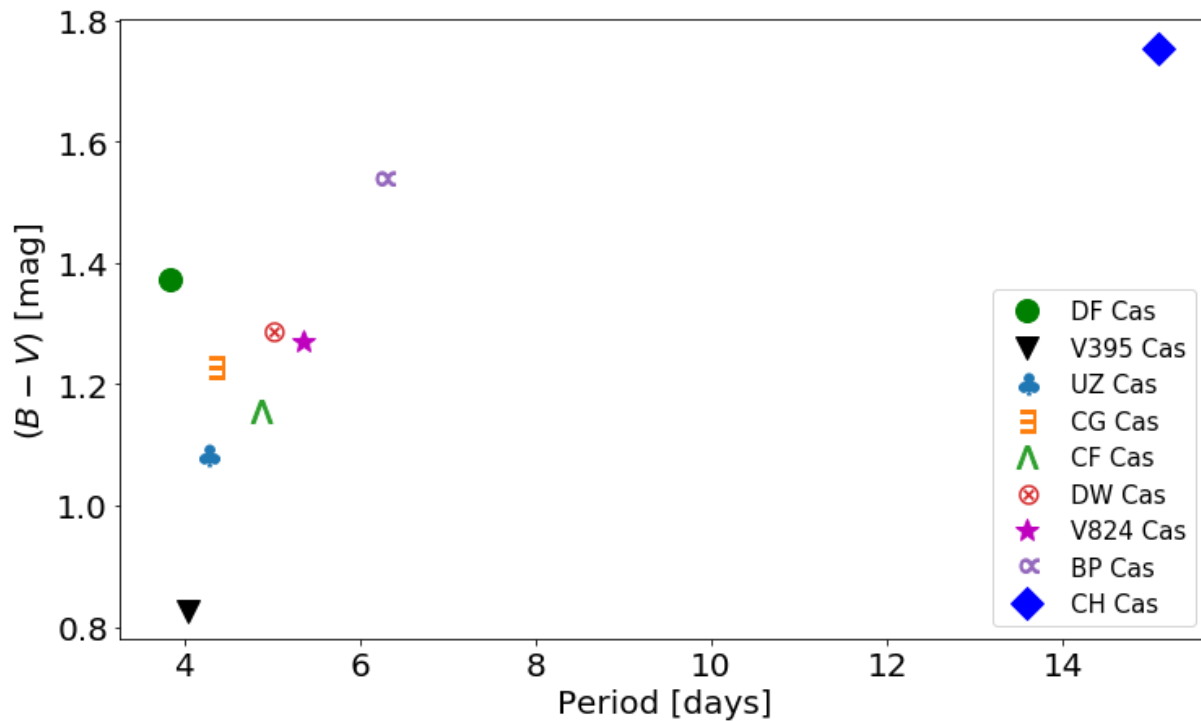Table 3.1: Variable stars information. Taken from the VSX database.

Figure 3.1: Period distribution vs *(B-V)* color index for selected Cepheid.

3.2 The methodology of choosing control and check stars

By using the method of differential photometry, the brightness of a variable star is compared with the brightness of a control star. Often it is the case that additional stars (check stars) are chosen to make sure that the control star is not a variable star itself. The atmospheric and color extinction can be neglected because it is almost identical for all used stars due to their proximity on the sky.

Stars were being awarded points based on proximity from the variable star, a value of (*B-V*) color index relative to the variable star and the magnitude in *V* filter relative to the variable star. We have used the UCAC4 catalog (Zacharias, Finch, Girard, et al., 2013)[2] through the ALADIN software.

After awarding points, 5 stars with the most points were chosen and visually checked that they are not blended. A star with the most points was selected as a control star. Stars with the second and third most points were selected as check 1 and check 2 stars respectively.

Due to large vignetting, an emphasis was put on the selection of control stars that allows to put variable and comp stars close to the center of the chip. The chip of the G4-16000 CCD camera mounted at MUO contains bad columns. During the selection process, it was needed to avoid any positioning of variable or control stars near this stripe (Fig. 3.3). Star charts of variable, control and check stars can be found in Appendix A.

3.3 Observing at MUO

Observing of all selected Cepheids was carried out at MUO in Brno. The Table 3.2 shows in how many nights each star was observed and the number of frames gathered for each star in each filter. A sequence of two frames in *BVRI* filters was performed before moving to another target. Altogether, 7132 frames[3] were obtained during 25 nights. MUO is equipped with Newtonian 600/2780 mm telescope and G4-16000 peltier cooled CCD camera with *BVRI* filters manufactured by Moravian Instruments. Binning 2x2 was used in all frames to reduce the size of the frame file as well as the readout time.

Observations were carried out from late September 2017 to early March 2018. Twenty-three observing nights were done by Jiri Zak and 2 observing nights were done by Dr. Ernst Paunzen. Observing time in different nights varied from 9 hours to 1 hour. Due to the air mass, only stars that were higher than $30°$ were observed.

All obtained frames were dark and flat field frame corrected using CMUNIPACK (Motl, 2011). The aperture photometry was also performed in CMUNIPACK. In Figures 3.2 and 3.3, examples of frames before and after application of the correction frames are shown.

---

[2]http://www.usno.navy.mil/USNO/astrometry/optical-IR-prod/ucac
[3]including 1412 dark frames and 84 flat field frames.

Star	# of nights	B	V	R	I
DF Cas	12	237	237	237	237
V395 Cas	10	150	150	150	150
UZ Cas	13	143	143	143	143
CG Cas	15	165	165	165	165
CF Cas	15	165	165	165	165
DW Cas	8	143	143	143	143
V824 Cas	11	101	101	101	101
BP Cas	11	184	184	184	184
CH Cas	13	121	121	121	121

Table 3.2: Observation log with number of frames in each filter.
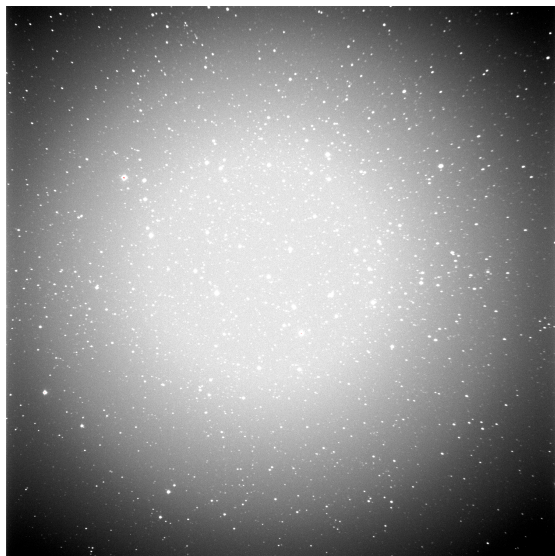
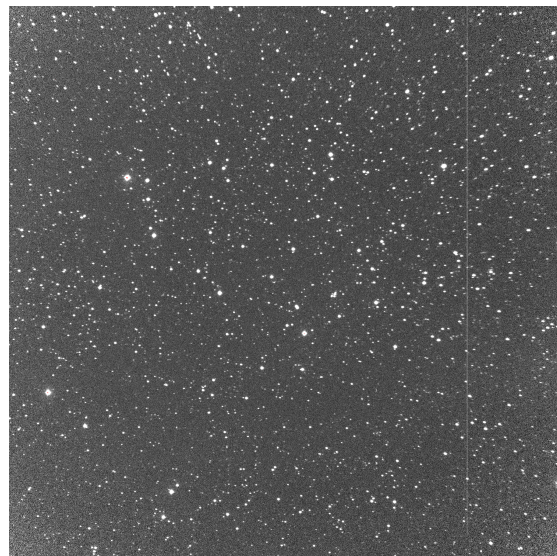Figure 3.2: Raw frame suffering from apparent vignetattion.

Figure 3.3: Dark and flat field corrected frame. There is a bad column visible on the right side of the frame.

At the beginning of the program, there was an attempt to create observing schedule of the Cepheids according to their periods such that each star would have the same number of observations per one pulsation cycle. However, this way was found unfeasible. It was not desirable to have only 2 or 4 frames per filter from the night as a very small number of data points per night makes choosing the proper aperture for data reduction very challenging.

As it turned out, it was more prudent to only select from 2 to 6 stars per night according to the current observability. This allowed denser data coverage and obtaining more frames per night, which results in more comfortable data reduction and outlier detection. In the later stage of this project, it also allowed for easier phase gap filling.

3.4   Standard system coefficients

The star field containing CF and CG Cas also contained a star cluster NGC 7790. This star cluster has been well observed by Henden (1999) and has been used to perform calibration to the standard system. The same data reduction process as for Cepheids using CMUNIPACK was performed in case the of NGC 7790. The procedure that was used for obtaining standard system coefficients is described in section 2.5. Obtained coefficients are presented in Table 3.3. From these values, it can be seen that all filters are almost identical to the standard ones.

$C_B=$	(0.96 ± 0.02)	$k_1=$	(0.03 ± 0.01)
$C_V=$	(-0.05 ± 0.05)	$k_2=$	(0.03 ± 0.01)
$C_R=$	(-1.06 ± 0.05)	$k_3=$	(0.04 ± 0.01)
$C_I=$	(-0.97 ± 0.03)	$k_4=$	(0.04 ± 0.02)

Table 3.3: Obtained calibration coefficients.

(a) C_B coefficient

(b) C_V coefficient

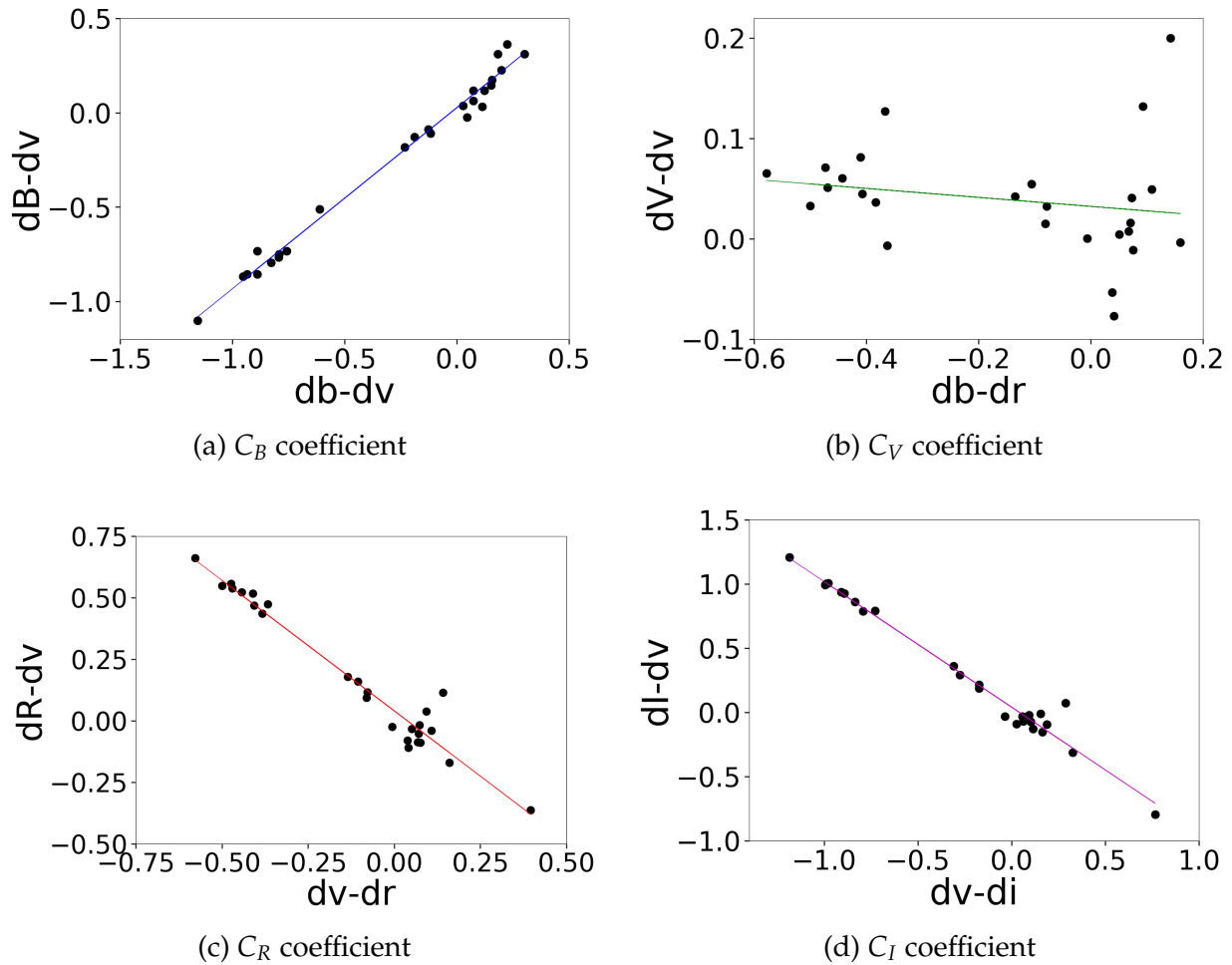(c) C_R coefficient

(d) C_I coefficient

Figure 3.4: Interrelation between MUO system and standard system. The solid lines show linear fits to the data.

Chapter 4

Results

4.1 Phase curves

In the following sections, phase curves of observed Cepheids are presented. In all figures that show the phase curve models, Fourier fit (Eq. 2.6) of the fourth order was used as it performed well in the visual test. A dependency of the Fourier coefficients on the order of the fit has been tested on DF Cas in *B* filter (see Fig. B1 in the Appendix). As one can see in Table B1 in the Appendix, the order of the fit does not dramatically change the Fourier coefficient values.

As can be seen in the following sections, the amplitude is the largest in the *B* filter and gradually decreases as we move towards longer wavelengths. This is an expected result which applies to all Cepheids and has been well observed before. Modified Julian Day (MJD) is used to express phasing moments for better readability in all plots showing phase curves. MJD is defined as follows

$$\text{MJD} = \text{HJD} - 2400000.5, \tag{4.1}$$

where HJD is a Heliocentric Julian Day. Period *P* and epoch phasing moment *M* are presented at the top of each graph containing phase curve models.

4.1.1 DF Cas

DF Cas has the shortest period from the selected sample. This allowed obtaining one of the best coverages of the phase curve. Both minima and maxima are covered as well as ascending and descending branches (Fig. 4.1). No special light-curve features were identified. In Table 4.1 Fourier coefficients of DF Cas are presented.
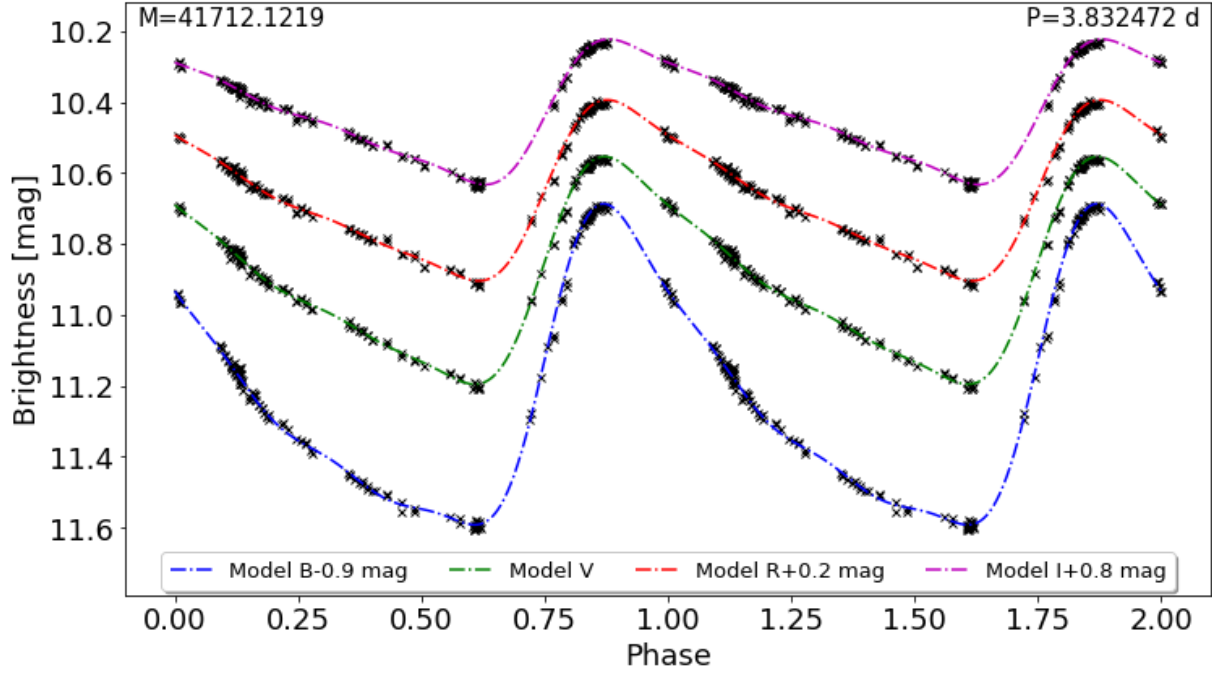
Figure 4.1: Phase curves of DF Cas.

	A_0 [mag]	A_1 [mag]	R_{21}	R_{31}	R_{41}
B	12.133(1)	0.386(2)	0.843(5)	0.385(4)	0.155(5)
V	10.906(1)	0.265(1)	0.713(5)	0.400(4)	0.151(5)
R	10.469(1)	0.209(1)	0.650(7)	0.406(6)	0.156(7)
I	9.631(1)	0.166(1)	0.530(7)	0.409(5)	0.169(6)

	ϕ_1 [rad]	ϕ_{21} [rad]	ϕ_{31} [rad]	ϕ_{41} [rad]
B	0.075(6)	2.508(17)	5.228(30)	1.643(63)
V	0.067(6)	2.805(17)	5.807(33)	2.340(65)
R	10.068(8)	2.861(22)	5.911(44)	2.510(87)
I	0.086(8)	3.040(21)	6.195(40)	3.011(61)

Table 4.1: Fourier coefficients for DF Cas.

4.1.2 V395 Cas

Despite having the second shortest period from the selected sample of Cepheids, the ascending branch of V395 Cas is not covered well. However, the maximum and descending branch are covered well (Fig. 4.2). In Table 4.2 Fourier coefficients of V395 Cas are presented.
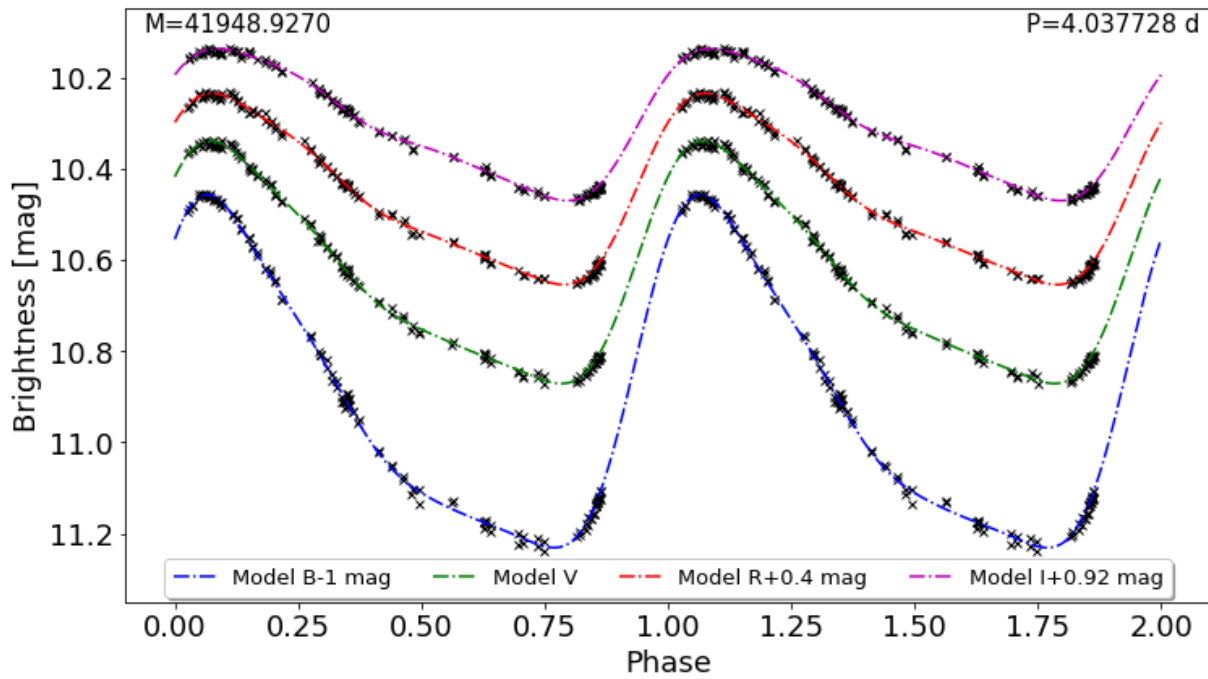

Figure 4.2: Phase curves of V395 Cas.

	A_0 [mag]	A_1 [mag]	R_{21}	R_{31}	R_{41}
B	11.918(1)	0.352(2)	0.320(4)	0.121(4)	0.036(4)
V	10.644(1)	0.237(1)	0.340(4)	0.118(4)	0.042(4)
R	10.064(1)	0.186(1)	0.338(5)	0.114(5)	0.046(5)
I	9.388(1)	0.147(1)	0.339(5)	0.104(6)	0.048(5)

	ϕ_1 [rad]	ϕ_{21} [rad]	ϕ_{31} [rad]	ϕ_{41} [rad]
B	3.609(4)	2.374(18)	5.369(43)	1.43(14)
V	3.509(5)	2.518(19)	5.626(46)	1.91(13)
R	3.431(6)	2.664(23)	5.949(58)	2.29(14)
I	3.311(7)	2.858(25)	0.101(65)	2.84(15)

Table 4.2: Fourier coefficients for V395 Cas.

4.1.3 UZ Cas

UZ Cas is one of the best-observed Cepheids from our sample. Both maxima and min-ima are well covered as well as ascending and descending branches. Small wiggle on the descending branch of the model curve (around phase 0.75) can be seen in Fig. 4.3. This is most likely due to the inaccuracies and lack of the data rather than due to any physical phenomena.
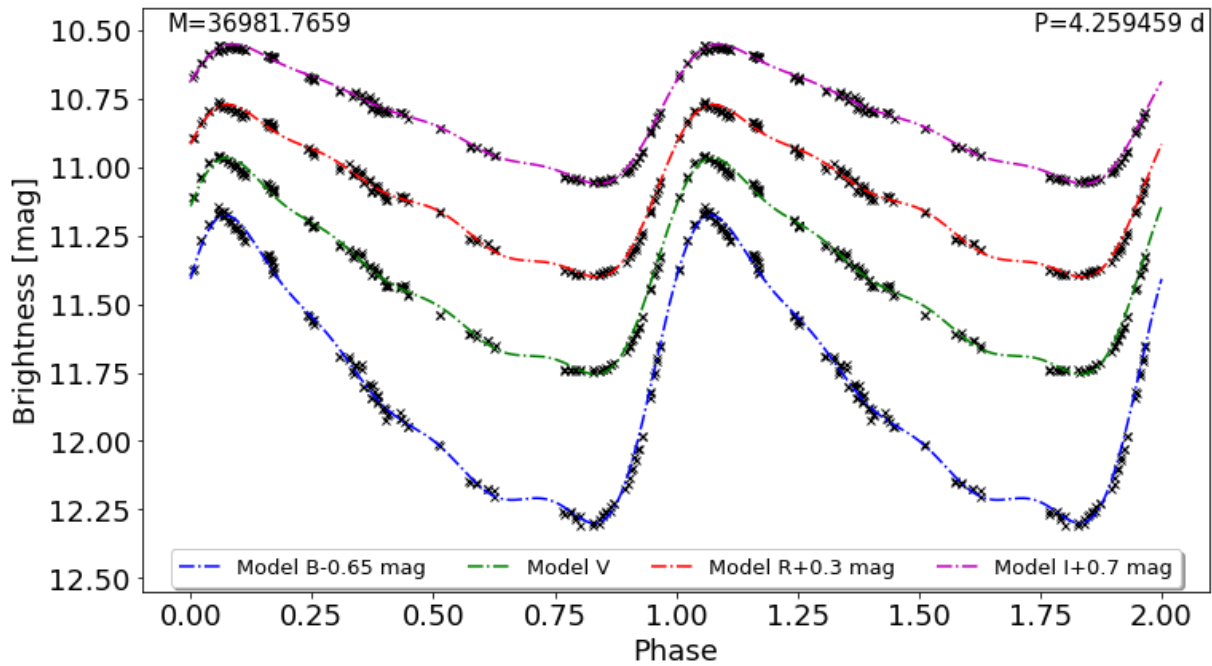

Figure 4.3: Phase curves of UZ Cas.

	A_0 [mag]	A_1 [mag]	R_{21}	R_{31}	R_{41}
B	12.488(3)	0.474(4)	0.371(7)	0.184(10)	0.104(7)
V	11.415(2)	0.330(3)	0.374(8)	0.181(10)	0.108(8)
R	10.814(2)	0.264(3)	0.373(9)	0.168(11)	0.119(8)
I	10.117(1)	0.211(2)	0.378(8)	0.175(10)	0.092(8)

	ϕ_1 [rad]	ϕ_{21} [rad]	ϕ_{31} [rad]	ϕ_{41} [rad]
B	2.276(7)	2.609(29)	5.327(42)	2.074(73)
V	2.184(7)	2.820(33)	5.570(47)	2.312(77)
R	2.100(8)	3.013(35)	5.778(56)	2.666(79)
I	2.029(7)	3.035(33)	5.943(53)	2.955(90)

Table 4.3: Fourier coefficients for UZ Cas.

4.1.4   CG Cas

CG Cas has been observed frequently, however, ascending branch has not been observed (Fig. 4.4). Many observations are near maxima region and on the descending branch. Thus the precise location of the minima and its height cannot be measured well. Further observations are needed in order to better determine the amplitude.
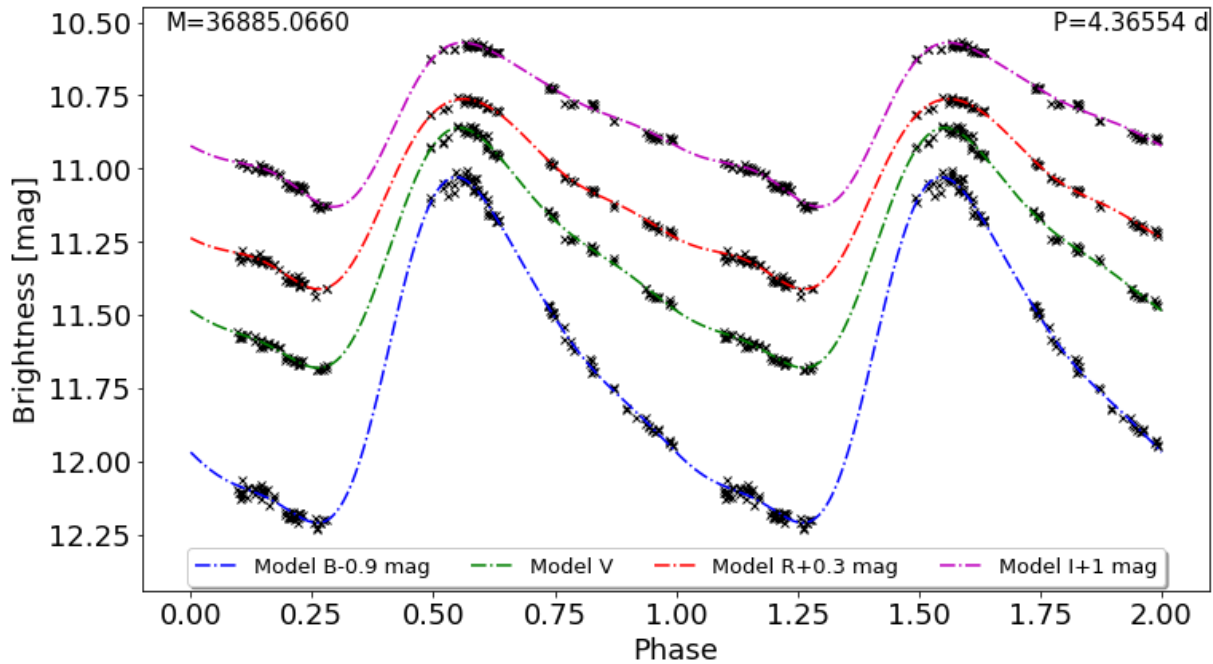

Figure 4.4: Phase curves of CG Cas.

	A_0 [mag]	A_1 [mag]	R_{21}	R_{31}	R_{41}
B	12.605(4)	0.514(3)	0.359(7)	0.126(7)	0.037(5)
V	11.317(3)	0.349(2)	0.367(7)	0.135(7)	0.022(6)
R	10.807(3)	0.275(2)	0.375(8)	0.115(8)	0.045(8)
I	9.850(3)	0.223(2)	0.421(11)	0.178(10)	0.057(8)

	ϕ_1 [rad]	ϕ_{21} [rad]	ϕ_{31} [rad]	ϕ_{41} [rad]
B	1.025(14)	2.605(42)	5.340(75)	2.48(23)
V	0.961(14)	2.729(41)	5.498(70)	3.01(38)
R	0.943(16)	2.729(45)	5.761(90)	3.76(17)
I	0.742(20)	2.974(53)	6.122(84)	3.70(23)

Table 4.4: Fourier coefficients for CG Cas.

4.1.5 CF Cas

CF Cas is another example of well-covered Cepheid from our sample. It has equally covered phase curve (Fig. 4.5). Fourier fit does not show any systematic deviation from our data.

	A_0 [mag]	A_1 [mag]	R_{21}	R_{31}	R_{41}
B	12.369(1)	0.365(2)	0.330(6)	0.094(5)	0.303(5)
V	11.104(1)	0.237(1)	0.326(6)	0.114(6)	0.056(5)
R	10.628(1)	0.193(1)	0.328(7)	0.100(7)	0.034(6)
I	9.718(1)	0.155(1)	0.281(6)	0.127(6)	0.044(5)

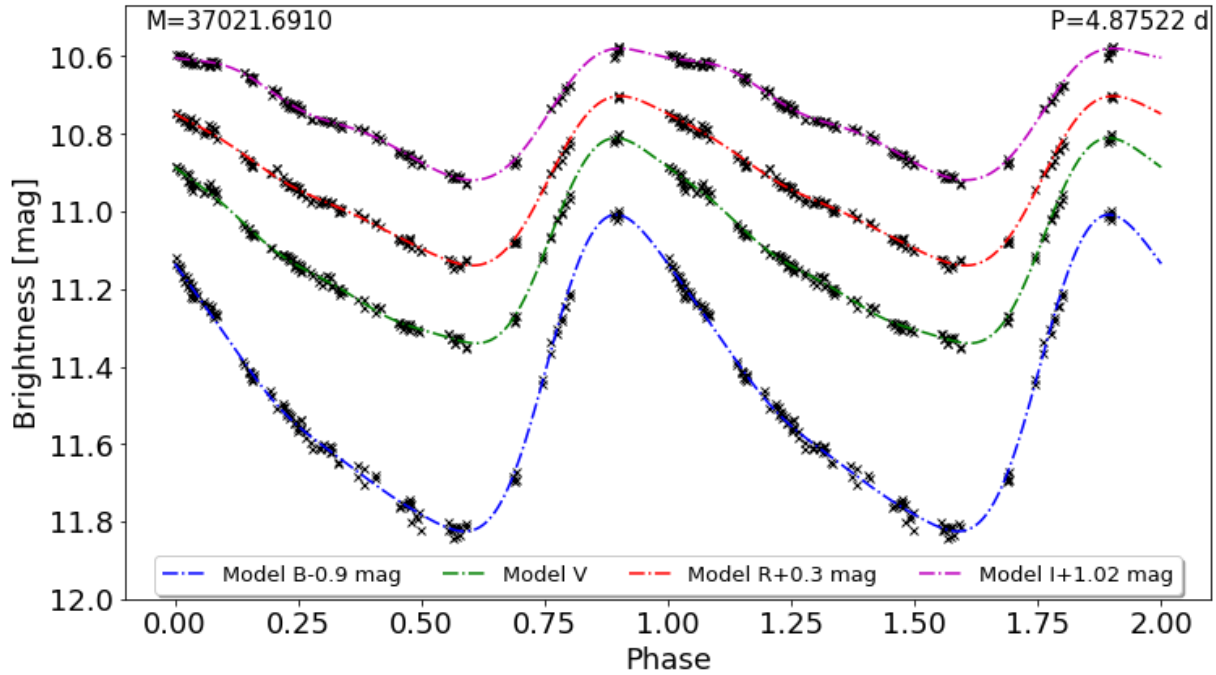|	ϕ_1 [rad]	ϕ_{21} [rad]	ϕ_{31} [rad]	ϕ_{41} [rad]
B	2.212(5)	2.634(16)	5.587(56)	2.02(17)
V	2.120(5)	2.759(18)	5.722(49)	2.349(98)
R	2.031(6)	2.964(21)	6.238(67)	2.59(18)
I	1.886(6)	3.284(21)	0.706(44)	2.61(13)

Table 4.5: Fourier coefficients for CF Cas.

Figure 4.5: Phase curves of CF Cas.

4.1.6 DW Cas

DW Cas is quite noticeable as it has period almost equal to 5 days. This has caused that the star was always observed in the same five phases (see Fig. 4.6). This prevented the full coverage of the phase curve during the observing season. The minimum light region and final part of the ascending branch are covered well.
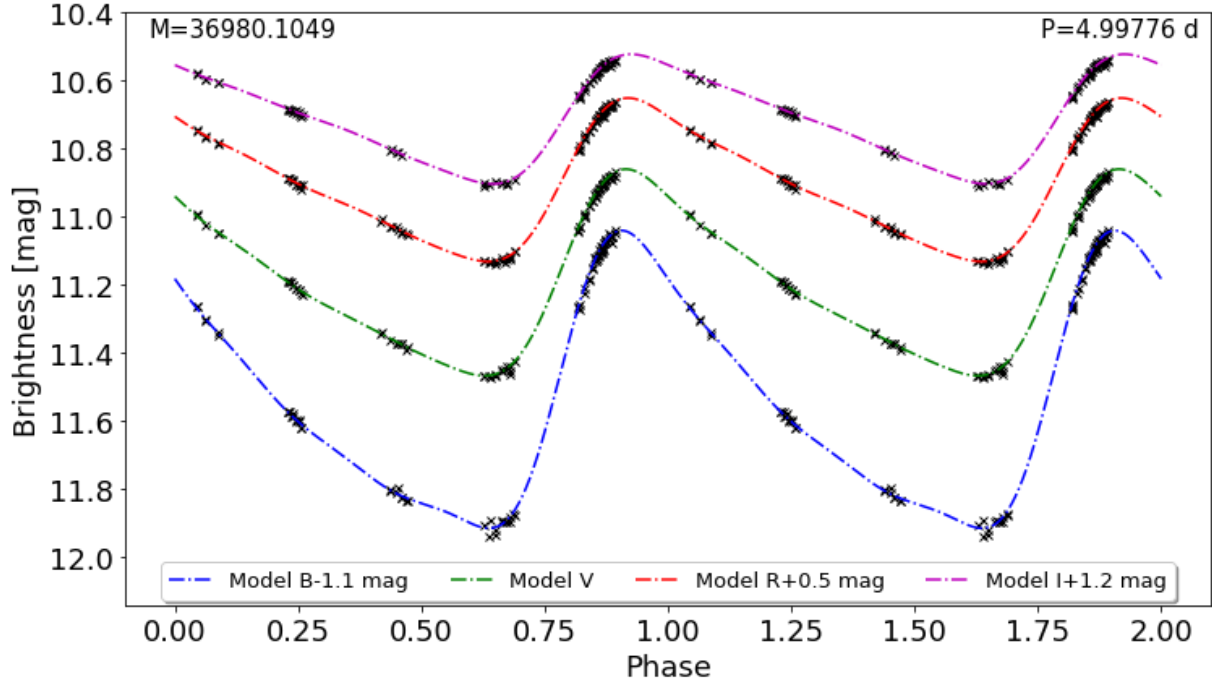
Figure 4.6: Phase curves of DW Cas.

	A_0 [mag]	A_1 [mag]	R_{21}	R_{31}	R_{41}
B	12.647(1)	0.375(4)	1.173(11)	0.367(13)	0.150(13)
V	11.197(1)	0.259(2)	1.083(7)	0.364(10)	0.133(8)
R	10.407(1)	0.203(2)	0.991(8)	0.37(11)	0.131(9)
I	9.514(1)	0.162(2)	0.887(17)	0.364(16)	0.128(20)

	ϕ_1 [rad]	ϕ_{21} [rad]	ϕ_{31} [rad]	ϕ_{41} [rad]
B	0.056(11)	2.637(37)	5.429(70)	1.99(17)
V	0.041(8)	2.823(24)	5.702(64)	1.99(18)
R	0.044(8)	2.990(26)	5.935(73)	2.31(18)
I	0.044(17)	3.174(63)	6.23(0.11)	2.94(26)

Table 4.6: Fourier coefficients of DW Cas.

4.1.7   V824 Cas

Coverage of phase curves for V824 Cas is satisfactory. No major gaps are present (Fig. 4.7). It was found that the period listed in the VSX database differs from the actual value. A better period was estimated using All Sky Automated Survey for Supernovae data (ASAS-SN, Shappee, Prieto, Stanek, et al., 2014; Kochanek, Shappee, Stanek, et al., 2017)[1]. More details about ASAS-SN can be found in sect. 4.3.1. The PERSEA software (Maciejewski, 2007, based on the algorithm by Schwarzenberg-Czerny (1996)) was used to estimate a new period as $P = 5.3506 \pm 0.0009$ days. This calculation was based on 553 data points in time range of 1108 days. A comparison of the original and new period is presented in Fig. 4.8. Periodogram is shown in Figure B2 in the Appendix.
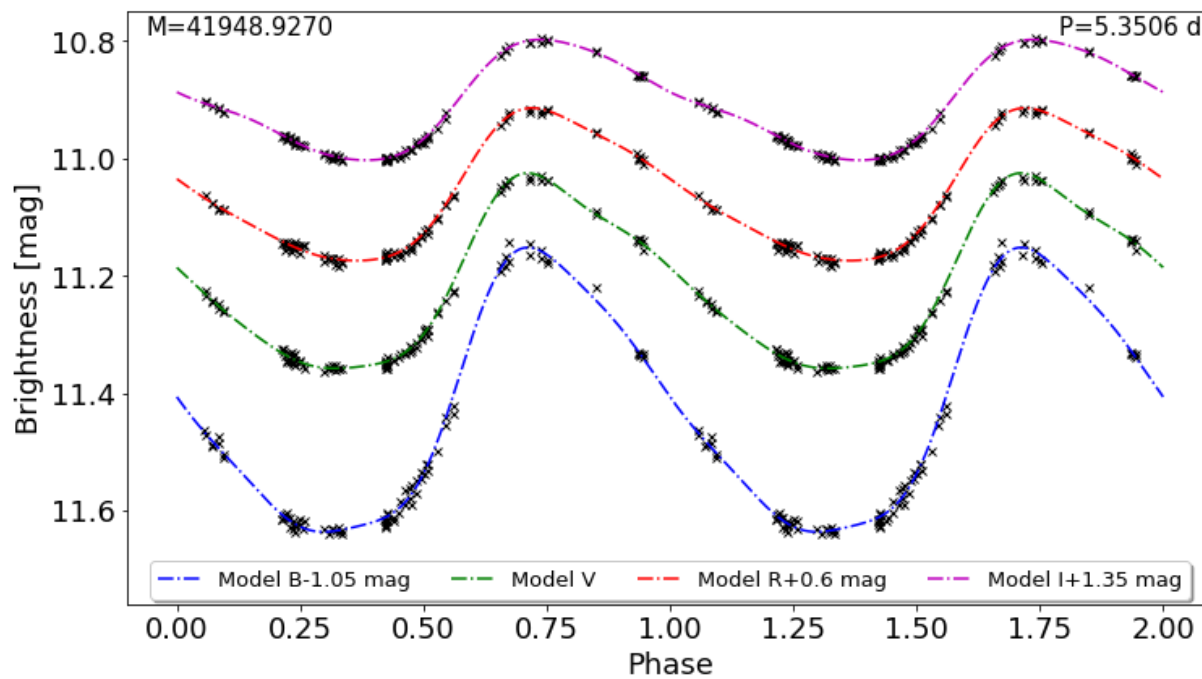
Figure 4.7: Phase curves for V824 Cas.

	A_0 [mag]	A_1 [mag]	R_{21}	R_{31}	R_{41}
B	12.475(2)	0.235(2)	0.204(8)	0.085(13)	0.043(11)
V	11.213(1)	0.159(1)	0.214(6)	0.111(9)	0.041(7)
R	10.456(1)	0.124(1)	0.229(7)	0.080(10)	0.033(9)
I	9.554(1)	0.097(1)	0.262(6)	0.036(7)	0.037(8)

	ϕ_1 [rad]	ϕ_{21} [rad]	ϕ_{31} [rad]	ϕ_{41} [rad]
B	4.798(8)	2.615(54)	5.234(89)	1.89(21)
V	4.742(6)	2.780(37)	5.365(57)	1.65(19)
R	4.695(8)	2.829(41)	5.617(86)	1.88(26)
I	4.607(6)	3.006(29)	5.99(15)	2.69(15)

Table 4.7: Fourier coefficients of V824 Cas.
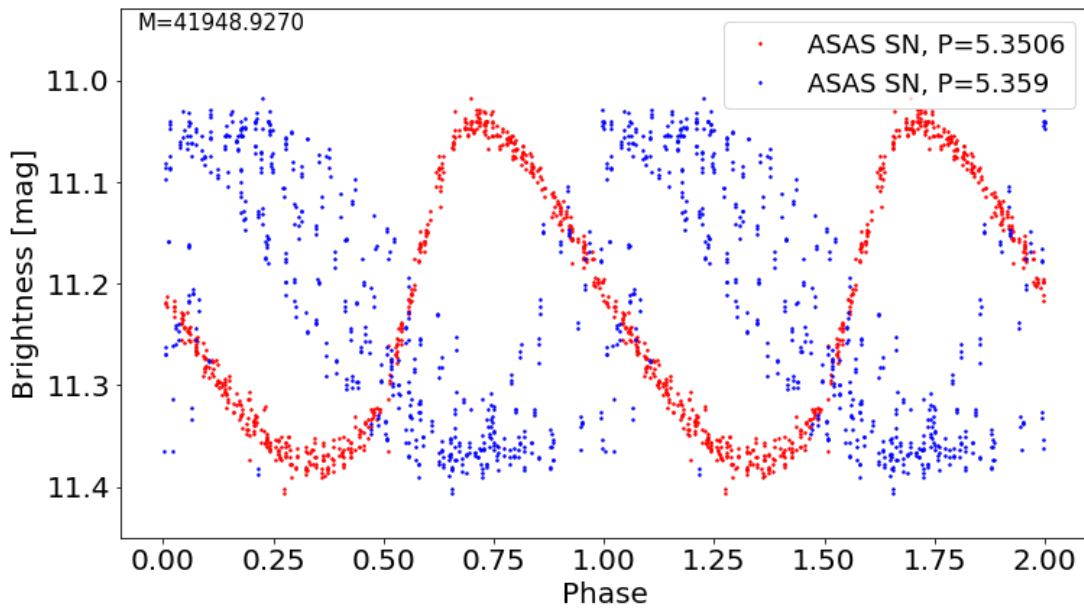
Figure 4.8: Comparison of the ASAS-SN data phased with former and newly determined period. The same zero epoch as in Fig. 4.7 was used.

4.1.8   BP Cas

Phase coverage of BP Cas is adequate. Except for the upper part of the ascending branch, every part of the phase curve is covered (Fig. 4.9). BP Cas shows the bump on the descending branch (around phase 0.15). Possible explanations of this phenomenon are mentioned in section 1.3.3. This bump has been observed during two nights and also subsequently confirmed by data obtained from the ASAS-SN archive, which clearly shows that it is not an instrumental artefact, but a real feature (Fig. 4.10).
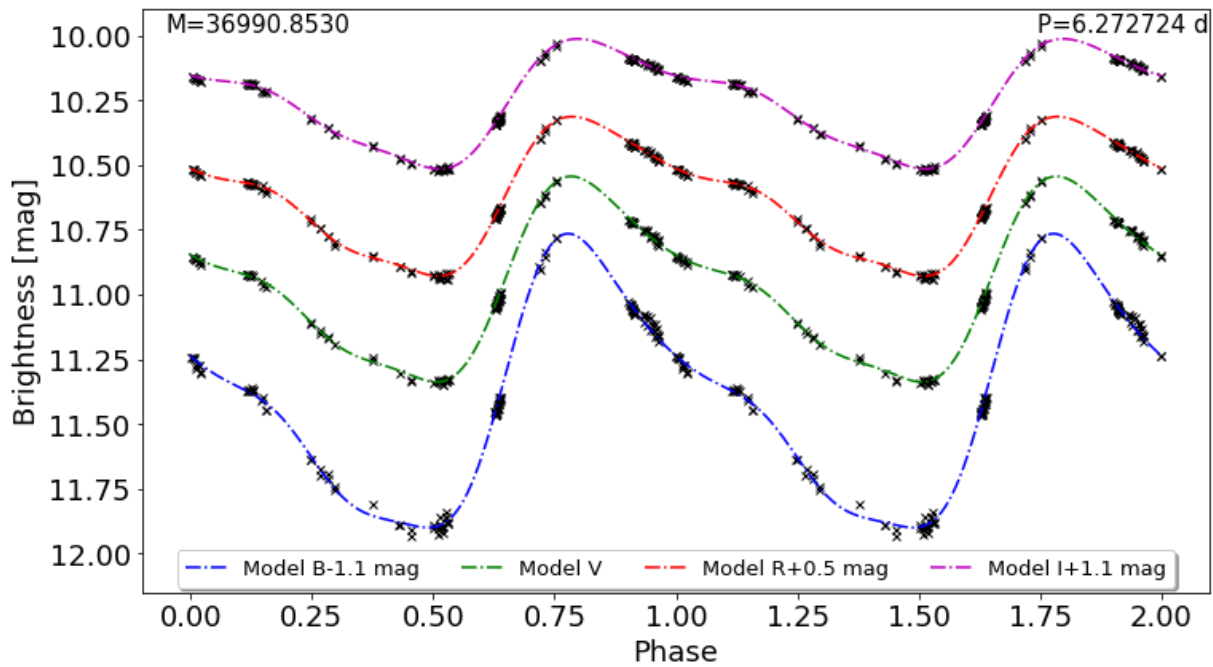

Figure 4.9: Phase curves for BP Cas.

	A_0 [mag]	A_1 [mag]	R_{21}	R_{31}	R_{41}
B	12.502(2)	0.491(4)	0.364(6)	0.136(6)	0.051(10)
V	10.970(1)	0.335(2)	0.382(5)	0.150(4)	0.049(8)
R	10.126(1)	0.264(1)	0.370(4)	0.136(4)	0.065(7)
I	9.156(1)	0.214(1)	0.368(5)	0.144(5)	0.043(7)

	ϕ_1 [rad]	ϕ_{21} [rad]	ϕ_{31} [rad]	ϕ_{41} [rad]
B	-1.840(5)	3.041(23)	5.294(47)	2.53(10)
V	-1.293(4)	3.130(16)	5.561(32)	3.135(71)
R	-1.375(4)	3.321(15)	5.791(31)	3.557(51)
I	-1.477(5)	3.481(17)	6.101(33)	4.19(11)

Table 4.8: Fourier coefficients of BP Cas.
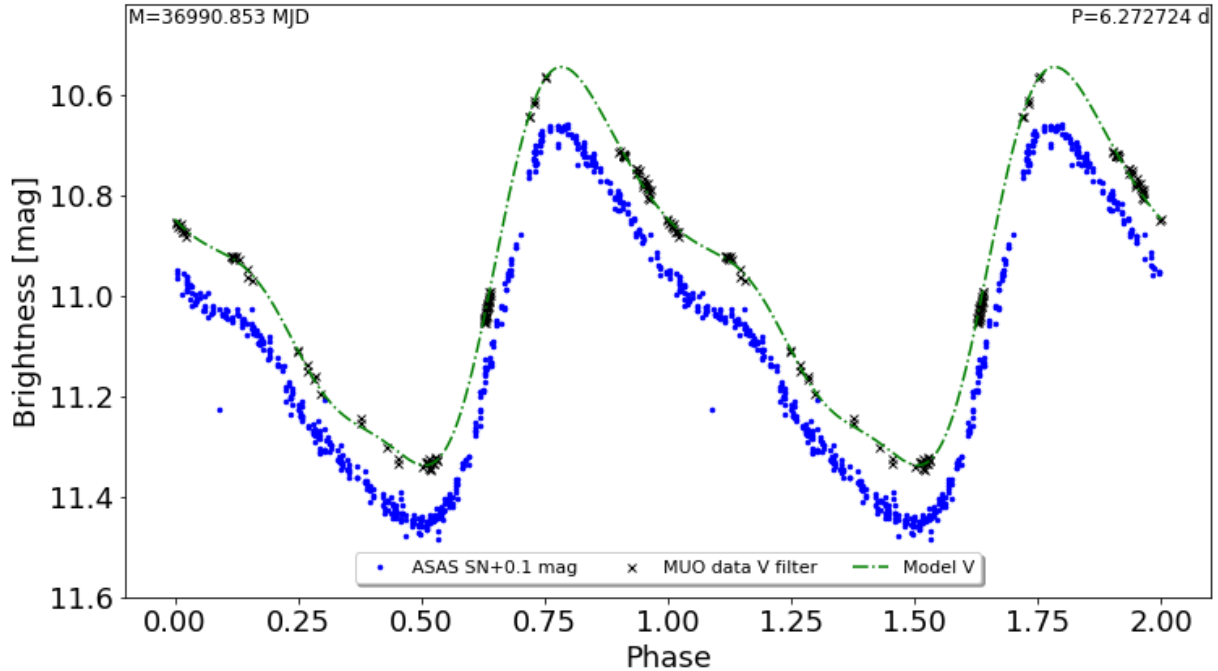
Figure 4.10: Comparison of ASAS-SN data and MUO *V* filter data for BP Cas.

4.1.9   CH Cas

CH Cas has the longest period from the selected sample. This, together with the period close to integer of 15 days, resulted in a poor coverage of the phase curve despite being observed during twelve nights (see Fig. 4.11). Another obstacle with CH Cas was that it sets below 30° as one of the first and was unobservable shortly after sunset in February and March. Fourier fit was performed, however, the model shows shortcomings as the minimum was not observed. CH Cas has the largest amplitude from the sample of Cepheids.
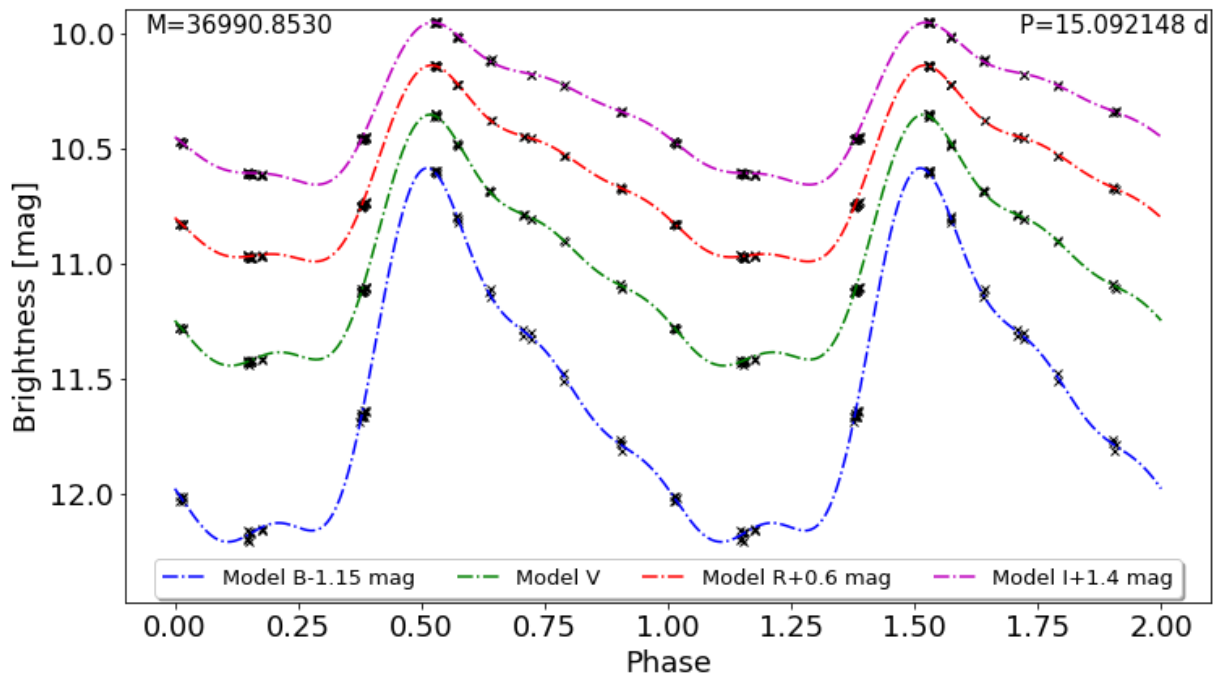
Figure 4.11: Phase curves of CH Cas.

	A_0 [mag]	A_1 [mag]	R_{21}	R_{31}	R_{41}
B	12.752(5)	0.671(7)	0.358(18)	0.208(9)	0.133(12)
V	11.019(3)	0.454(5)	0.345(17)	0.212(6)	0.138(11)
R	10.044(2)	0.359(3)	0.354(12)	0.206(5)	0.123(9)
I	8.945(2)	0.292(4)	0.362(16)	0.206(7)	0.117(12)

	ϕ_1 [rad]	ϕ_{21} [rad]	ϕ_{31} [rad]	ϕ_{41} [rad]
B	0.328(14)	2.625(34)	4.98(10)	1.38(12)
V	0.226(13)	2.809(31)	5.139(95)	1.712(98)
R	0.134(9)	2.996(23)	5.449(69)	2.074(85)
I	0.032(11)	3.176(28)	5.784(92)	2.53(12)

Table 4.9: Fourier coefficients for CH Cas.

4.2 Discussion on the light curve parameters

From Figs. 4.1-4.7, 4.9, 4.11 and 4.12, it is apparent that the amplitude of the light curve is clearly wavelength dependent as it increases towards shorter wavelengths. Since the effective wavelength of the filter determines the depth of the observed layer, it can be seen that the layers with higher temperature have larger amplitude of brightness changes compared to the cooler layers.

Fig. 4.12 shows that the amplitude is slowly increasing with increasing period. Amplitudes in all filters are listed in Table 4.10. The actual amplitude of CH Cas is most likely higher as neither the maximum or minimum was observed (Figure 4.11). V824 Cas exhibits unexpectedly low values of the amplitude for all filters. The unusually low amplitude of V824 Cas brings up the question whether the Cepheid is correctly classified.

Star name	B Amp. [mag]	V Amp. [mag]	R Amp. [mag]	I Amp. [mag]
DF Cas	0.91	0.64	0.51	0.41
V395 Cas	0.77	0.53	0.42	0.33
UZ Cas	1.13	0.79	0.63	0.51
CG Cas	1.18	0.82	0.65	0.56
CF Cas	0.82	0.53	0.44	0.34
DW Cas	0.87	0.61	0.48	0.38
V824 Cas	0.48	0.33	0.26	0.21
BP Cas	1.13	0.79	0.62	0.50
CH Cas	1.62	1.09	0.85	0.70

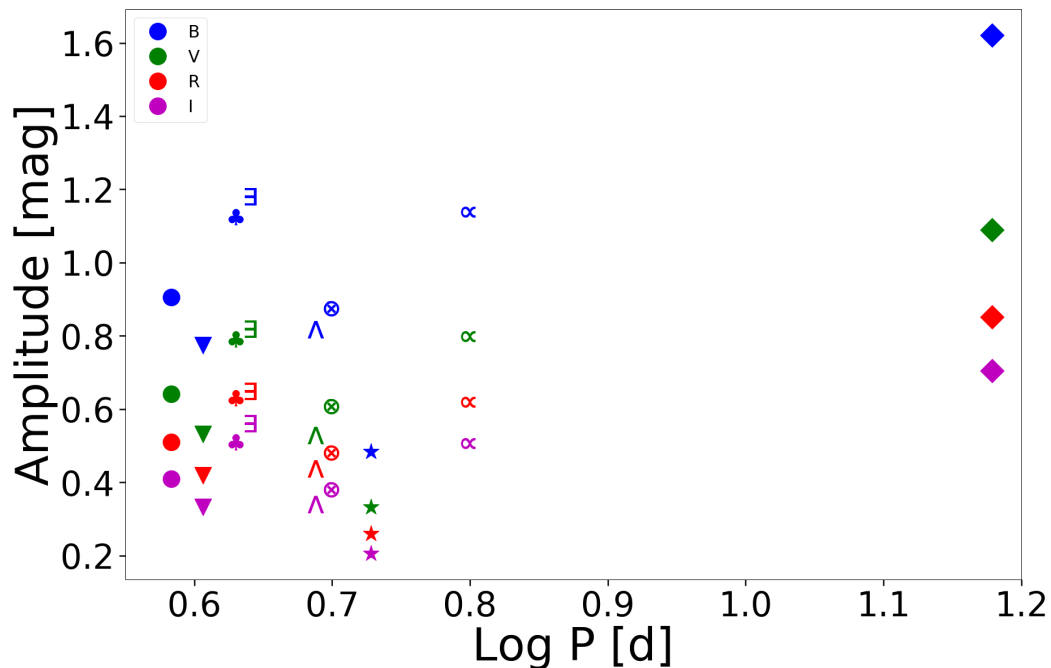Table 4.10: Light-curve amplitudes of selected Cepheids.

Figure 4.12: Light-curve amplitude dependency on the logarithm of the period for all filters. Symbols for the stars are the same as in Fig. 3.1.

A special class of Cepheids, so-called s-Cephei (sometimes called DCEPS) are Delta Cephei variables with light amplitude below 0.5 mag in *V* (0.7 mag in *B*) and almost symmetrical light curves, their period is usualy lower than $P < 7$ d. Most likely they are first overtone pulsators. According to these characteristics, V824 Cas could possibly be classified as s-Cepheid.

A methodology described in a paper by Antonello, Poretti, & Reduzzi (1990) gives two suitable criteria to distinguish s-Cepheids from their normal amplitude relatives using Fourier parameters. S-Cepheids should form a lower sequence below the normal amplitude Cepheids sequence in the R_{21} versus period plot. Another criterium was postulated as the s-Cepheids should form an upper sequence above the normal amplitude Cepheids in the ϕ_{31} versus period plot. It can be seen in Figure 4.16 that the first criterium is met, however, the second criterium has failed (Fig. 4.15). Thus, the classification of V824 Cas as s-Cepheid is not conclusive.

Another explanation of the unusual amplitude can be a binarity status. Binarity plays a relevant role when investigating the observable amplitudes of Cepheids, as more than 50% of Galactic Cepheids belong to binary or multiple systems (Szabados, 2003). The presence of a companion can affect the photometric amplitudes and cause a reduction of the observable amplitude of the brightness variation due to a presence of a constant source of light. This was used in a paper by Coulson & Caldwell (1989) on the sample of Cepheids to hint a possibility of a hidden companion for Cepheids that

deviate from a constant trend. As shown by Tanvir (1997) the amplitude ratio A_I/A_V is not dependent on the period and has a constant value of $A_I/A_V \sim 0.64$.

In Figure 4.13, the amplitude ratio A_I/A_V can be seen for Cepheids observed at MUO. The largest deviation shows CG Cas which is a known spectroscopic binary (Szabados, 1996). The second largest deviation from mean value exhibits V824 Cas. This might imply the presence of a companion. This finding deserves further, more complex, both photometric and spectroscopic investigation. It is worth to mention that a visual check of the vicinity of V824 Cas did not show any nearby star that could affect the amplitude.

Amplitude dependency on the wavelength results in clear dependency and systematics of ϕ_{21} and ϕ_{31} in different filters (Figs. 4.14 and 4.15). However, amplitude coefficitents R_{21} and R_{31} lack this dependency (Figs. 4.16 and 4.17).

Period dependencies of obtained coefficients are in good agreement with the progressions predicted by Bhardwaj, Kanbur, Marconi, et al. (2017). Coefficient ϕ_{21} shows clear rise with increasing period from $\log(P) \sim 0.6$ d to $\log(P) \sim 0.8$ d (Fig. 4.14). In Fig. 4.15, it can be seen that the coefficient ϕ_{31} is at expected plato which lasts from $\log(P) \sim 0.6$ d to $\log(P) \sim 0.8$ d.

The value of R_{21} is not changing much. An exception is V824 Cas which shows significantly lower values of this coefficient (Fig. 4.16). Parameter R_{31} is slightly decreasing with increasing period until $\log(P) \sim 0.8$ d. Again, V824 Cas shows unexpectedly low values (Fig. 4.17).
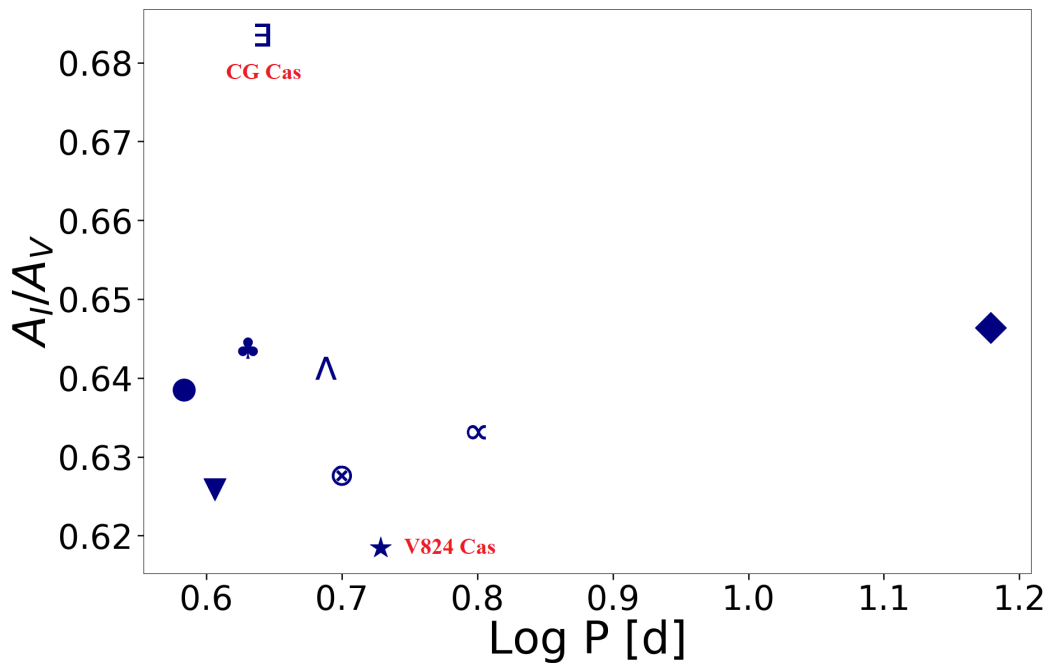

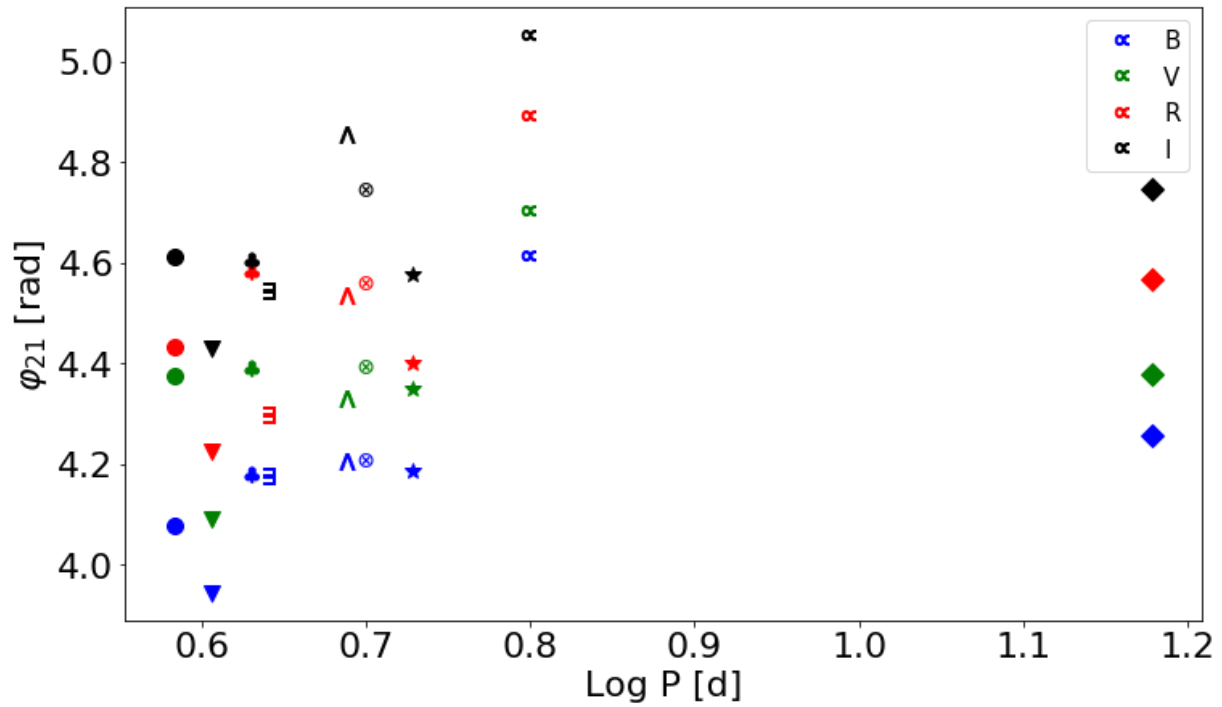Figure 4.13: Amplitude ratio A_I/A_V. Symbols for the stars are the same as in Fig. 3.1.

Figure 4.14: Obtained ϕ_{21} coefficients in different filters. Symbols for the stars are the same as in Fig. 3.1.
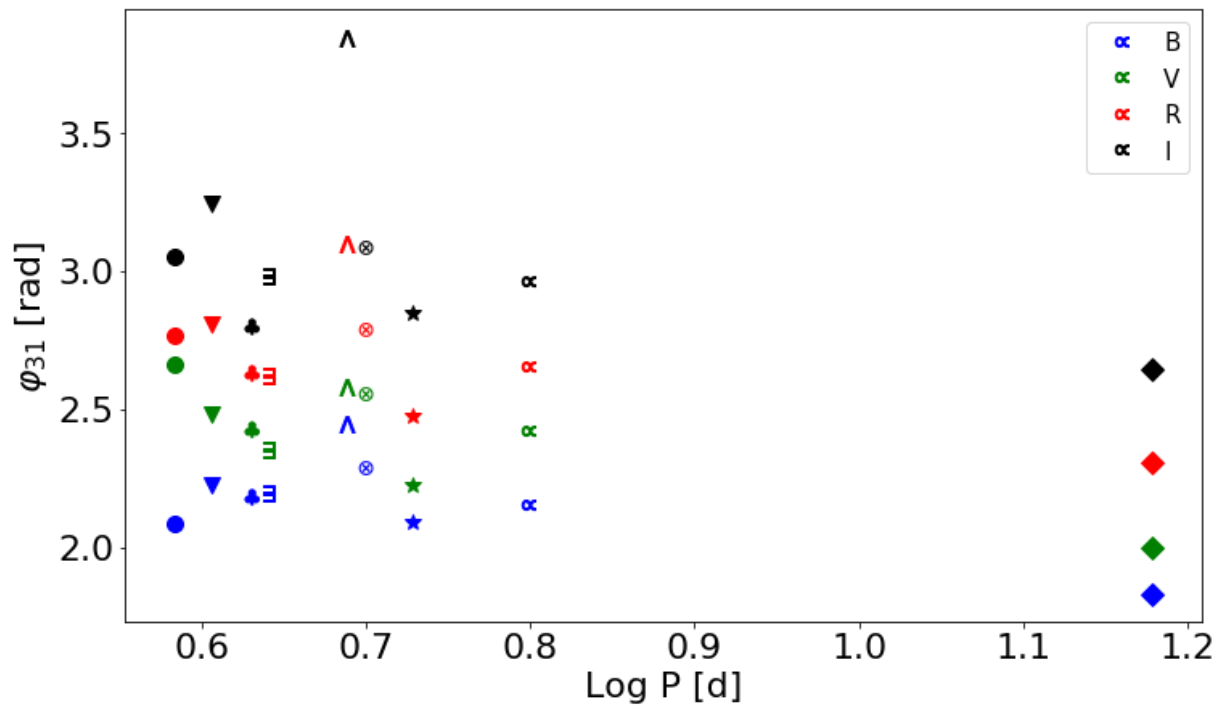

Figure 4.15: The same as in Fig. 4.14, but for ϕ_{31}.

Figure 4.16: The same as in Fig. 4.14, but for R_{21}.

Figure 4.17: The same as in Fig. 4.14, but for R_{31}.

4.3 Comparison with the data from other sources

4.3.1 Comparison with ASAS-SN and NITRO database

ASAS-SN is a program targeted to search for new supernovae and other transients (Shappee, Prieto, Stanek, et al., 2014; Kochanek, Shappee, Stanek, et al., 2017). It covers both northern and southern hemispheres. It measures objects with magnitude between 8 and 18 in the V filter. First two units consist of eight 14-cm telescopes. Photometric data for our analysis were obtained from https://asas-sn.osu.edu/ website and Fourier coefficients were subsequently calculated using the fourth order fit in CEPHEUS.

Nitro[2] database (Morgan, 2003) contains data and Fourier coefficients for over 1000 Galactic variables of which many are Cepheids. Several Cepheids from our sample are listed in their database. Data are in the V filter and are not from a single source for all the stars. Data sources are listed in Table B2 in the Appendix. Data from Berdnikov (2008) were added for V824 Cas as this star is not listed at the Nitro database.

The comparison shows a good agreement for the majority of the stars (Figs. 4.18-4.21). One of the common reasons for the data discrepancy of the compared coefficient is the sparse coverage of the phase curves of data acquired at MUO. This is most noticeably apparent in CG Cas (Fig. 4.4), DW Cas (Fig. 4.6) and CH Cas (Fig. 4.11). The discrepancy could also be caused by the different order of the Fourier fit and by the quality of the data from the literature. Data obtained at MUO are fitted with the fourth order polynomial. On the other hand, the order of the fit from Nitro database varies from the third to the seventh order. Another cause can originate from various time bases of acquired data sets. MUO data were obtained during roughly 6 months, ASAS-SN data were obtained during more than 30 months. These effects combined together preclude from obtaining exactly the same results.

The largest discrepancy in comparison shows CH Cas. As discussed above, there are many effects that can play role. However, because of near 15-day period of CH Cas, it is difficult to get well covered light curve (as can be seen from Fig. 4.11). This is most likely the reason why the coefficients from different sources differ. Since ASAS data has the best phase coverage, they are the most reliable.

DF Cas also displays slight discrepancy in each coefficient. This is probably caused by insufficient coverage of the minima and beginning of the ascending branch, however, there may be another reason as overall coverage of the phase curve is adequate. Distinct order of the fit was used as a database data were fitted by only third order function. No other star shows any major deviation in comparison.

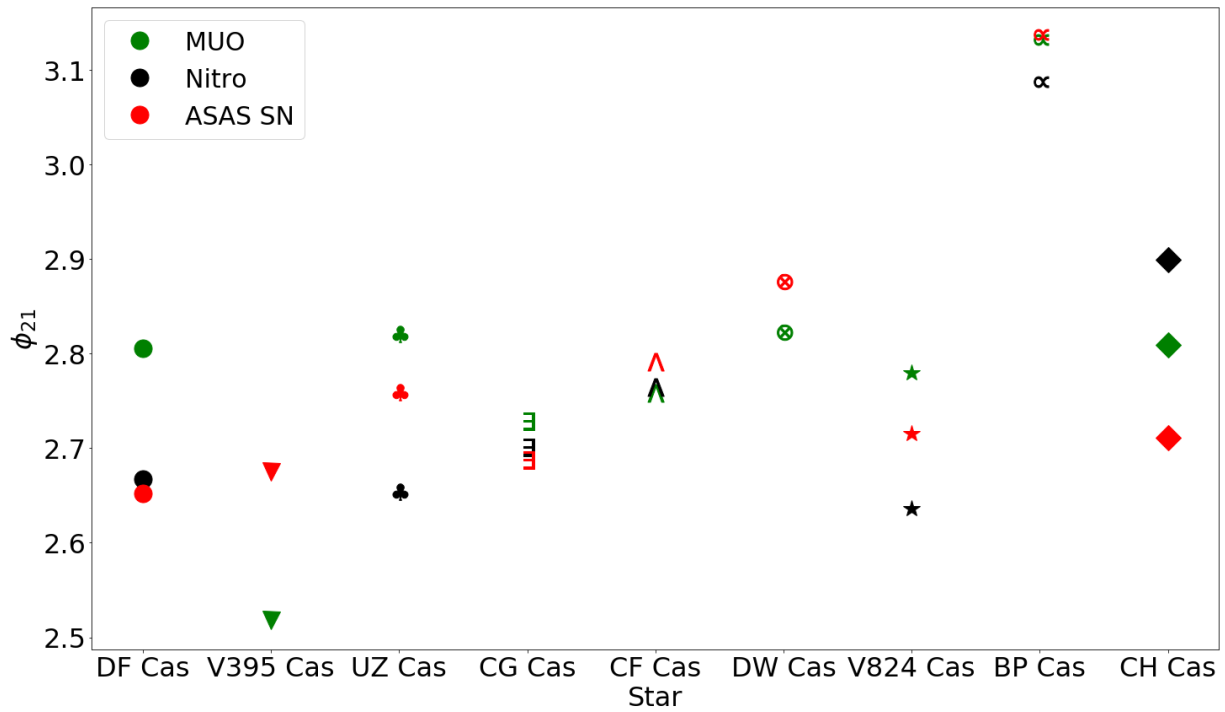---

[2]http://nitro9.earth.uni.edu/

Figure 4.18: Comparison of ϕ_{21} coefficient. Symbols for the stars are the same as in Fig. 3.1.
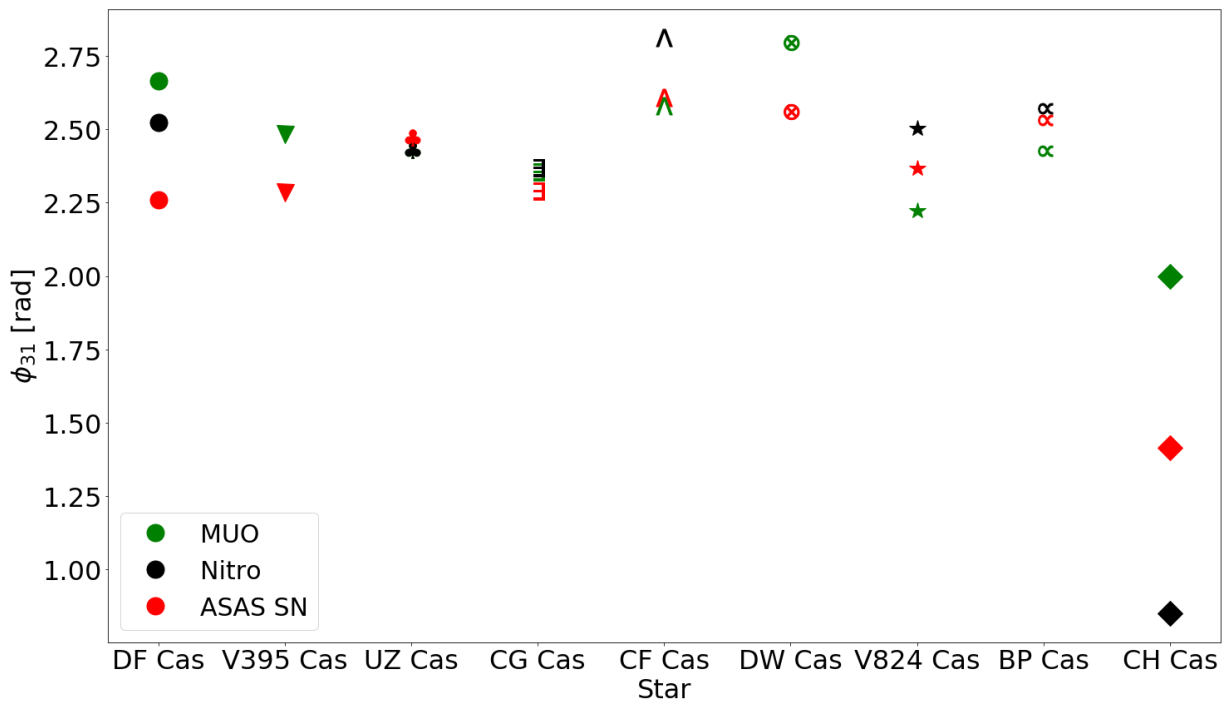

Figure 4.19: The same as in Fig. 4.18, but for ϕ_{31}.
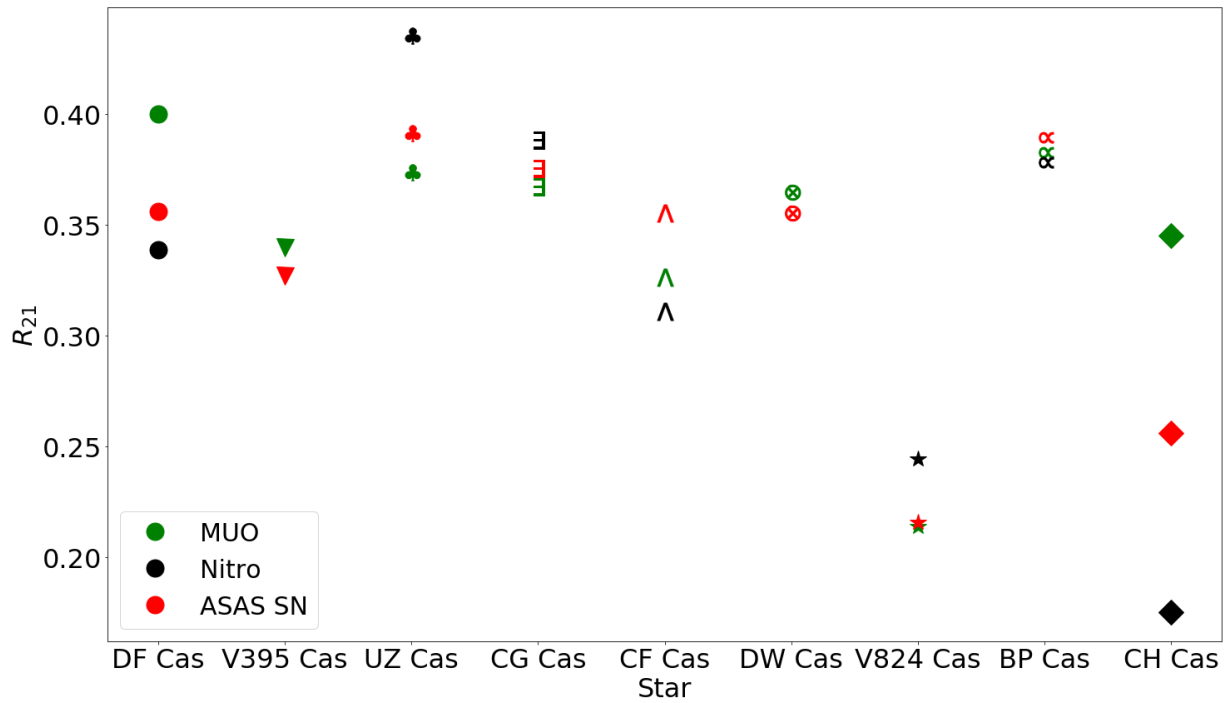
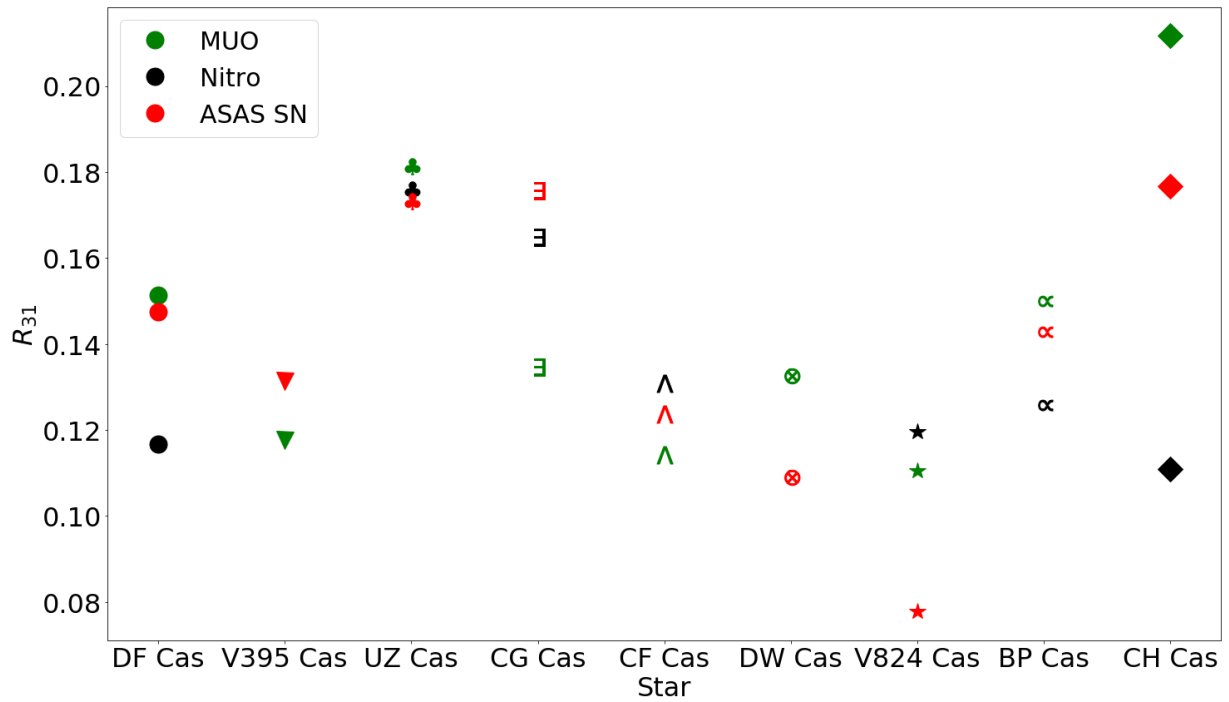Figure 4.20: The same as in Fig. 4.18, but for R_{21}.

Figure 4.21: The same as in Fig. 4.18, but for R_{31}.

4.3.2   Comparison with OGLE data

The Optical Gravitational Lensing Experiment (OGLE, Udalski, Szymański, Kaluzny, et al., 1992; Udalski, Szymański, & Szymański, 2015) is a sky survey with the main objective of searching for the dark matter with microlensing phenomena. The project is located at the Las Campanas Observatory in Chile. As a byproduct, it has discovered several exoplanets and created an enormous database of variable stars data. Main objects of interest are specifically the Magellanic Clouds and the Galactic Bulge. Soszyński, Udalski, Szymański, et al. (2015, 2017), have published an analysis of OGLE data and calculated Fourier coefficients for Cepheids in LMC, SMC and Galactic Bulge. In the forthcoming text, we compare Fourier coefficients in I filter from MUO and OGLE, because OGLE observations are made mostly in I filter[3]. The same markers for each star were used as originally in Figure 3.1.

We can see a good agreement for most of the stars (Figs. 4.22-4.25). V824 shows the largest deviation from the trends. The cause of the deviation towards lower values can have many origins. According to Bhardwaj, Kanbur, Marconi, et al. (2017), Fourier coefficients are metallicity dependent. Another cause can be the data uncertainty. However, literature data in Figures 4.18 and 4.21 show even lower values than data obtained at MUO for ϕ_{21} and R_{31}. This may be an indication that V824 Cas could really be a peculiar Cepheid. This star has not been thoroughly studied before hence would be worthy of further observing.

Another star that differs from the general trends is CF Cas which has higher values of ϕ_{31} (Fig. 4.23) and lower values of R_{21} (Fig. 4.24). Coefficients from the literature (section 4.3.1) show a good agreement with the ones obtained at MUO, thus, we can conclude that the higher values are of a physical origin and not rather caused by the data uncertainty.

A very interesting is the comparison of R_{31} coefficient in Figure 4.25 as there is a clear separation of Cepheids located in LMC, SMC, and Bulge. As can be seen in Figure 4.25, the value of the R_{31} coefficient decreases as the metallicity increases (LMC, SMC and Bulge have different metallicity). Data from MUO nicely fits in this sequence when solar metallicity $Z = 0.02$ is used. $Z_{SMC} = 0.004$ and $Z_{LMC} = 0.008$ values published in Glatt, Grebel, & Koch (2010) were used. Stars located in the Galactic Bulge span a metallicity range $-1.5 \lesssim [Fe/H] \lesssim 0.5$ (Barbuy, Chiappini, & Gerhard, 2018). This explains the wide spread of values for OGLE Bulge Cepheids in the diagram.
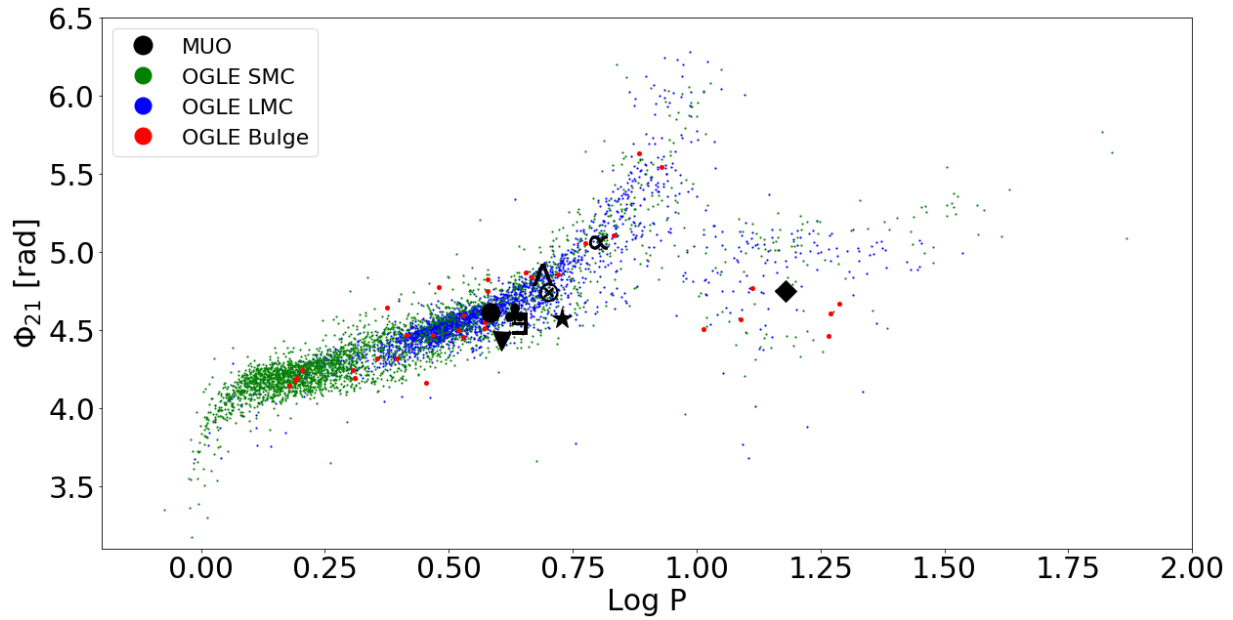
---

[3]Coefficient were obtained from ftp://ftp.astrouw.edu.pl/ogle4/OCVS/

Figure 4.22: Comparison of obtained φ_{21} Fourier coefficient with OGLE stars. Symbols for the stars are the same as in Fig. 3.1.
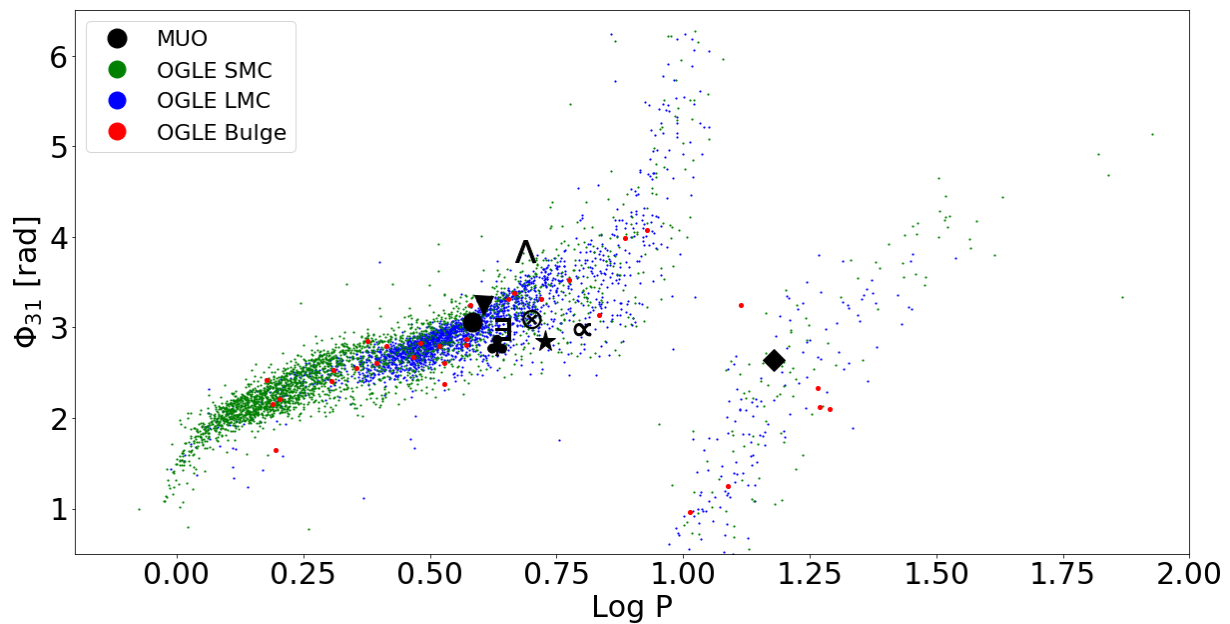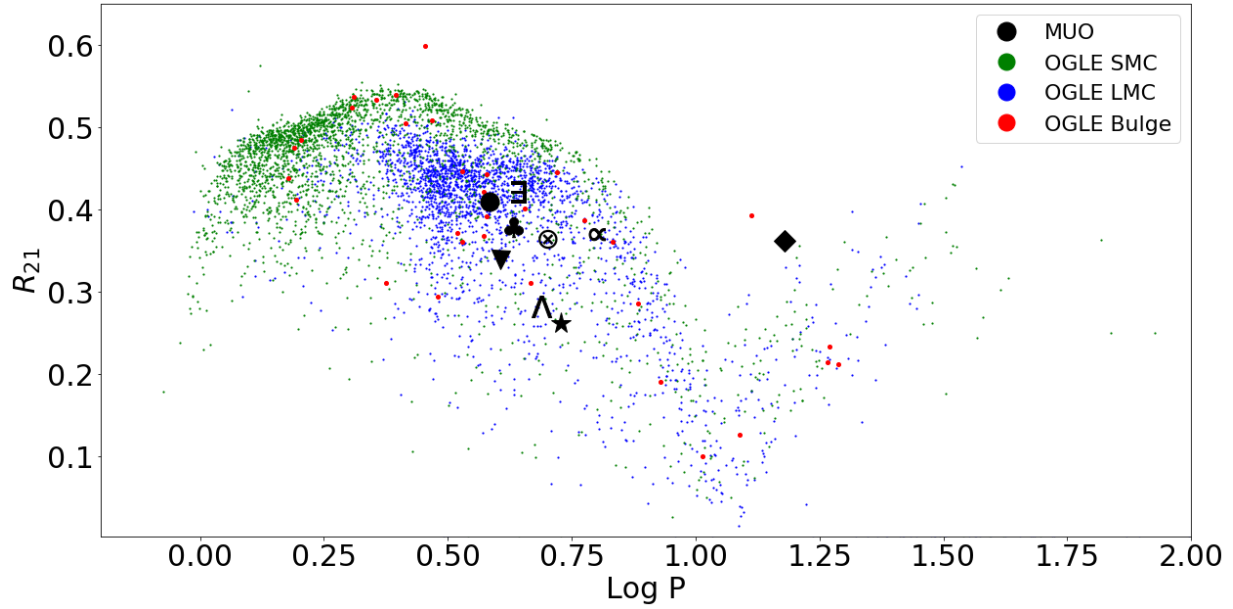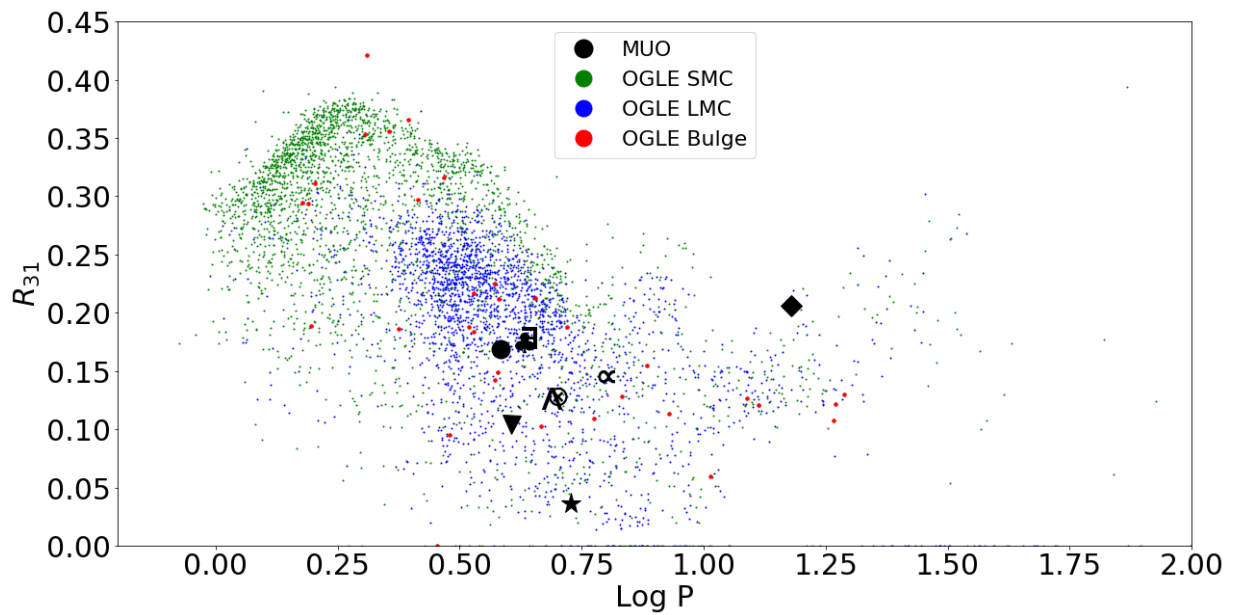

Figure 4.23: The same as in Fig. 4.22, but for ϕ_{31}.

Figure 4.24: The same as in Fig. 4.22, but for R_{21}.

Figure 4.25: The same as in Fig. 4.22, but for R_{31}.

Chapter 5

Conclussion

The goal of this project was to obtain original *BVRI* photometry of selected Galactic Cepheids and subsequent data reduction and analysis. Nine fundamental mode Cepheids from the Cassiopeia constellation (DF Cas, V395 Cas, UZ Cas, CG Cas, CF Cas, DW Cas, V824 Cas, BP Cas and CH Cas) were selected to be measured using the 600-mm telescope at Masaryk University Observatory in Brno, Czech Republic. Periods of selected Cepheids range from $P = 3.83$ days to $P = 15.09$ days. Set of *BVRI* Johnson-Cousins filters together with G4-16000 camera were used for the observations.

Measurements were carried out from late September of 2017 to mid-March of 2018. Altogether, 5636 data frames during 25 nights were acquired. The least number of frames (101) in each filter was gathered for V824 Cas, the most frames (237) was obtained for DF Cas. DW Cas was the least observed object with 8 observation nights. CF Cas and CG Cas were the most observed objects with 15 observation nights. NGC 7790 was used as a standard field for the transformation of the data to the standard system.

All data were fitted with Fourier polynomial of the fourth order to obtain Fourier coefficients. Phase coverage of the selected Cepheids varies and deteriorates with an increasing period. An estimation of a new period $P = 5.3506 \pm 0.0009$ days was performed for V824 Cas as the available database period was obsolete or not precise enough. The bump observed on the descending branch of the BP Cas was confirmed using ASAS-SN data and discussed in subsection 4.1.8.

The amplitude of the light curves shows clear dependency on the used filter as it increases towards shorter wavelengths. Fourier coefficients ϕ_{21} and ϕ_{31} display the inverse dependency as they decrease towards longer wavelengths. Coefficients R_{21} and R_{31} lack this dependency. This is in an agreement with the models published in the paper by Bhardwaj, Kanbur, Marconi, et al. (2017). CG Cas, as the only binary Cepheid in the sample, has the largest mean deviation in the A_I/A_V vs $\log P$ diagram (Fig. 4.13).

V824 Cas appears to have extraordinary low amplitude and amplitude Fourier coefficients. The later was confirmed by subsequent comparison of produced data to data available in Nitro database and to ASAS-SN data in the *V* filter. This unusual behavior may be caused by a binarity as this star deviates in Fig. 4.13 from the trend. This idea

47

is supported by the need for a new pulsation period estimation which could be caused by Light-Travel Time Effect as a consequence of an unseen companion orbiting the star. The period changes of this star deserve more thorough investigation. Another attempt to explain the low amplitude of V824 Cas is that it could possibly be of s-Cepheid type. However, after analyzing the Fourier coefficient, this claim has not been found conclusive. Another star that differs from the general trends is CF Cas. These stars are proposed for further investigation.

Coefficients from the Nitro database and data from ASAS-SN in the *V* filter were used to perform a comparison to the coefficient from MUO. All selected Cepheids, but CH and DF Cas, show a good agreement in the comparison and do not show any major systematic deviation. Deviation of the CH and DF Cas is most likely caused by a poor coverage of the phase curves. It was difficult to produce a good coverage of CH Cas as it has a pulsation period of $P = 15.09$ days. Coverage of the minima and beginning of the ascending branch was not obtained.

A comparison of the produced Fourier coefficients in the *I* filter to OGLE database is presented in section 4.3.2. OGLE observations of LMC, SMC and Galactic Bulge were used. In Figures 4.22, 4.23, 4.24 and 4.25 comparisons of the coefficients are presented. Parameter R_{31} shows an apparent separation for Cepheids from different systems (Fig. 4.25) as the value of the parameter decreases with increasing metallicity. This is in agreement with predictions published in Bhardwaj, Kanbur, Marconi, et al. (2017).

This project offers many opportunities for future work. Observed star fields contain over 40 known variables and provide a great opportunity to discover new ones. Observed star field containing NGC 7790 also contains visual binary Cepheid CE Cas a and CE Cas b. Their data were obtained and they are planned to be analysed in the future. Despite the fact that the number of CCD cameras and telescopes is increasing each year, there is still a need for further, mainly multicolor photometric and spectroscopic, observations of Cepheids to fully clarify and understand their behavior. A similar project with more selected Cepheids and better coverage of the phase curves would be an asset for the astronomical community. V824 Cas would benefit from further observation to clarify its peculiar behavior.

Bibliography

Antonello E., Morelli P. L., 1996, A&A, 314, 541

Antonello E., Poretti E., Reduzzi L., 1990, A&A, 236, 138

Barbuy B., Chiappini C., Gerhard O., 2018, arXiv, arXiv:1805.01142

Barnacka A., *Analiza danych fotometrycznych z przegladów "Pi of the sky" i ASAS*, Master Thesis, Kraków

Benedict G. F., McArthur B. E., Feast M. W., et al., 2007, AJ, 133, 1810

Berdnikov L. N., 2008, *VizieR Online Data Catalog: Photoelectric observations of Cepheids in UBV(RI)c*

Bessell M. S., 2005, ARA&A, 43, 293

Bhardwaj A., Kanbur S. M., Marconi M., et al., 2017, MNRAS, 466, 2805

Bonnarel F., Fernique P., Bienaymé O., et al., 2000, A&AS, 143, 33

Boyle W. S., Smith G. E., 1970, *Charge Coupled Semiconductor Devices*. Bell System Technical Journal, 49: 587-593

Catelan M., Smith H. A., 2015, *Pulsating stars*, Wiley-VCH, ISBN 978-3-527-40715-6

Cox J. P., 1980, *Theory of stellar pulsation*, Princeton University Press, ISBN 0691082537

Coulson I. M., Caldwell J. A. R., 1989, MNRAS, 240, 285

Eddington A. S., 1917, Obs, 40, 290

Eddington A. S., 1926, *The internal constitution of the stars*, Cambridge University Press, ISBN 0521337089

Fadeyev Y. A., 2014, AstL, 40, 301

Glatt K., Grebel E. K., Koch A., 2010, A&A, 517, A50

Glazebrook K., 2010, *Pulsating stars: Stars that breathe*, [online]
    http://astronomy.swin.edu.au/sao/downloads/HET611-M17A01.pdf

Hertzsprung E., 1926, BAN, 3, 115

Hertzsprung E., 1913, AN, 196, 201

Henden A., 1999, [online]
    http://binaries.boulder.swri.edu/fields/ngc7790.html

Johnson H. L., Morgan W. W., 1953, ApJ, 117, 313

Knapp J., 2011, *Lecture notes*, [online]
    https://www.astro.princeton.edu/~gk/A403/pulse.pdf

Kochanek C. S., Shappee B. J., Stanek K.Z., et al., 2017, PASP, 129, 104502

Kukarkin B. V., 1949, *Structure and evolution of stellar systems*, (Moscow: Government
    Printing Office)

Landolt A. U., 1983, AJ, 88, 439

Leavitt H. S., Pickering E. C., 1912, HarCi, 173, 1

Ledoux P., Walraven T., 1958, HDP, 51, 353

Maciejewski G., 2007, PERSEA, [online]
    http://www.astri.uni.torun.pl/

Madore B. F., Freedman W. L., 1991, PASP, 103, 933

Mikulášek Z., Zejda M., 2013, *Úvod do studia proměnných hvězd*, 213 s., ISBN 978-80-210-
    6241-2.

Moffett T. J., Barnes T. G., III, 1985, ApJS, 58, 843

Motl D., 2011, CMUNIPACK, [online]
    http://c-munipack.sourceforge.net/

Morgan S., 2003, Nitro database, [online]
    http://nitro9.earth.uni.edu/

Percy J. R., 2007, *Understanding the variable stars*, Cambridge University Press, ISBN
    1139463284

Plummer H. G., 1914, MNRAS, 74, 660

Postec N., 2012, *Pulsating stars: Stars that breathe*, [online]
    http://www.optique-ingenieur.org/en/courses/OPI_ang_M05_C06/co/   Con-
    tenu_13.html

Ritter A., 1879, AnP, 244, 157

Sandage A., 1958, ApJ, 127, 513

Santhanam P., Bhattacharyya J. C., 1985, KodOB, 5, 27

Simon N. R., Lee A. S., 1981, ApJ, 248, 291

Simon N. R., Schmidt E. G., 1976, ApJ, 205, 162

Schaltenbrand R., Tamman G., 1971, Astr. Ap. Suppl., 4, 265

Schwarzenberg-Czerny A., 1996, ApJ, 460, L107

Schwarzschild K., 1900, AN, 152, 65

Shapley H., 1914, ApJ, 40, 448

Shappee B., Prieto J., Stanek K.Z., et al., 2014, AAS, 223, 236.03

Soszyński I., Udalski A., Szymański M.K., et al., 2015, AcA, 65, 297

Soszyński I., Udalski A., Szymański M.K., et al., 2017, AcA, 67, 297

Szabados L., 1996, A&A, 311, 189

Szabados L., 2003, IBVS, 5394, 1

Tanvir N. R., 1997, eds..proc, 91

Udalski A., Szymański M., Kaluzny J., et al, 1992, AcA, 42, 253

Udalski A., Szymański M. K., Szymański G., 2015, AcA, 65, 1

Ulaczyk K., Szymański M. K., Udalski A., et al., 2013, AcA, 63, 159

Watson C. L., Henden A. A., Price A., 2006, SASS, 25, 47

Whitney C., 1956, AJ, 61, 192

Zacharias N., Finch C. T., Girard T. M., et al., 2013, AJ, 145, 44

Zhevakin S. A. , 1953, Russ A.J., 30, 161

Appendices

A Control stars info

Charts with marked variable, control, and check stars are provided in this section. Brief information about control and check stars is given. Data are taken from UCAC4 catalog using ALADIN software. The methodology of choosing control and checks stars used is described in detail in section 3.2. Star charts were created at https://www.aavso.org/apps/vsp/.

Catalog designation	V [mag]	$(B-V)$ [mag]
UCAC4 757-023315	10.29	1.335
UCAC4 757-023164	10.621	1.553
UCAC4 758-022984	11.626	1.116

Table A1: DF Cas control and check stars info.

Catalog designation	V [mag]	$(B-V)$ [mag]
UCAC4 767-020166	10.736	0.877
UCAC4 767-020248	11.221	0.665
UCAC4 767-020403	11.73	0.744

Table A2: V395 Cas control and check stars info.

Catalog designation	V [mag]	$(B-V)$ [mag]
UCAC4 757-012196	10.7	1.119
UCAC4 756-012441	10.836	1.003
UCAC4 758-012547	11.685	0.832

Table A3: UZ Cas control and check stars info.

As CG and CF Cas are quite similiar to each other as far as magnitude and (*B-V*) color index, this allowed us to choose one set of control stars for both variable stars.

Catalog designation	*V* [mag]	*(B-V)* [mag]
UCAC4 756-083283	11.704	1.435
UCAC4 757-080494	11.355	1.23
UCAC4 757-080554	10.576	1.3

Table A4: CG and CF Cas control and check stars info.

Catalog designation	*V* [mag]	*(B-V)* [mag]
UCAC4 748-086255	10.908	1.444
UCAC4 746-086987	10.95	1.385
UCAC4 747-084050	10.85	0.881

Table A5: DW Cas control and check stars info.

Catalog designation	*V* [mag]	*(B-V)* [mag]
UCAC4 765-005172	11.682	1.246
UCAC4 766-004539	10.765	1.271
UCAC4 766-004777	11.316	1.387

Table A6: V824 Cas control and check stars info.

Catalog designation	*V* [mag]	*(B-V)* [mag]
UCAC4 779-003306	11.535	1.556
UCAC4 777-004968	10.823	1.469
UCAC4 780-003802	11.362	1.531

Table A7: BP Cas control and check stars info.

Catalog designation	V [mag]	$(B\text{-}V)$ [mag]
UCAC4 764-071669	11.188	1.483
UCAC4 766-072427	11.138	1.676
UCAC4 765-073402	10.85	1.23

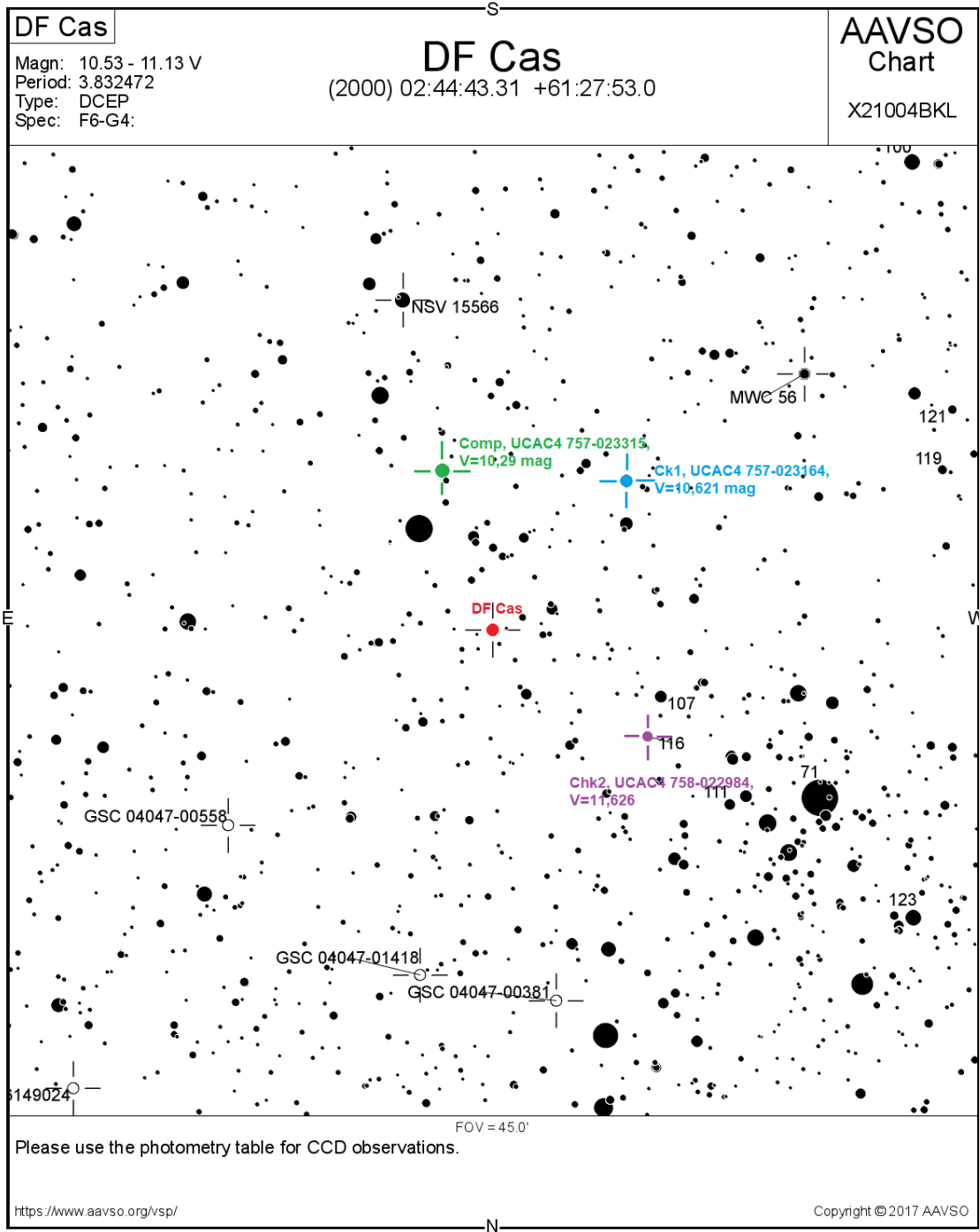Table A8: CH Cas control and check stars info.
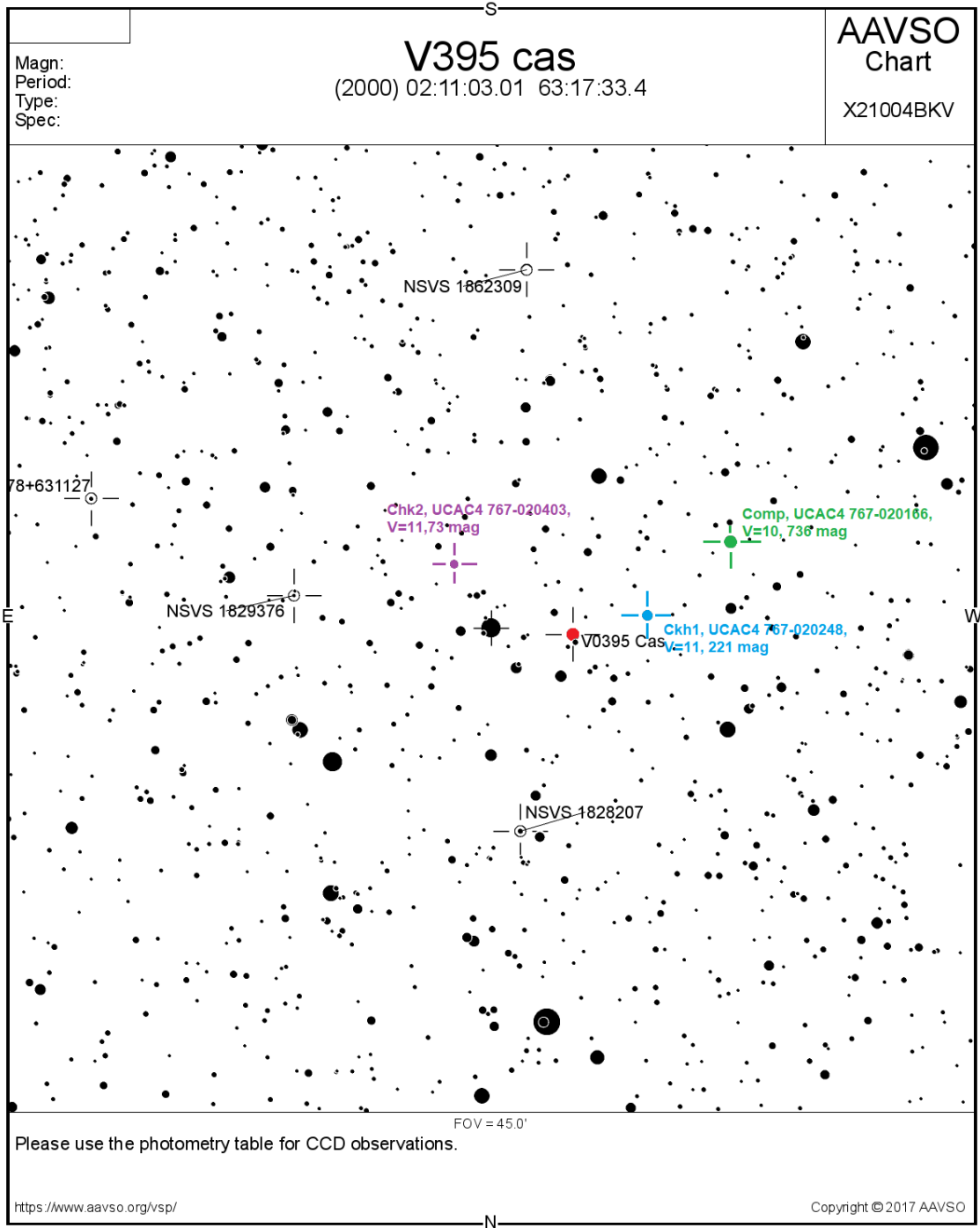
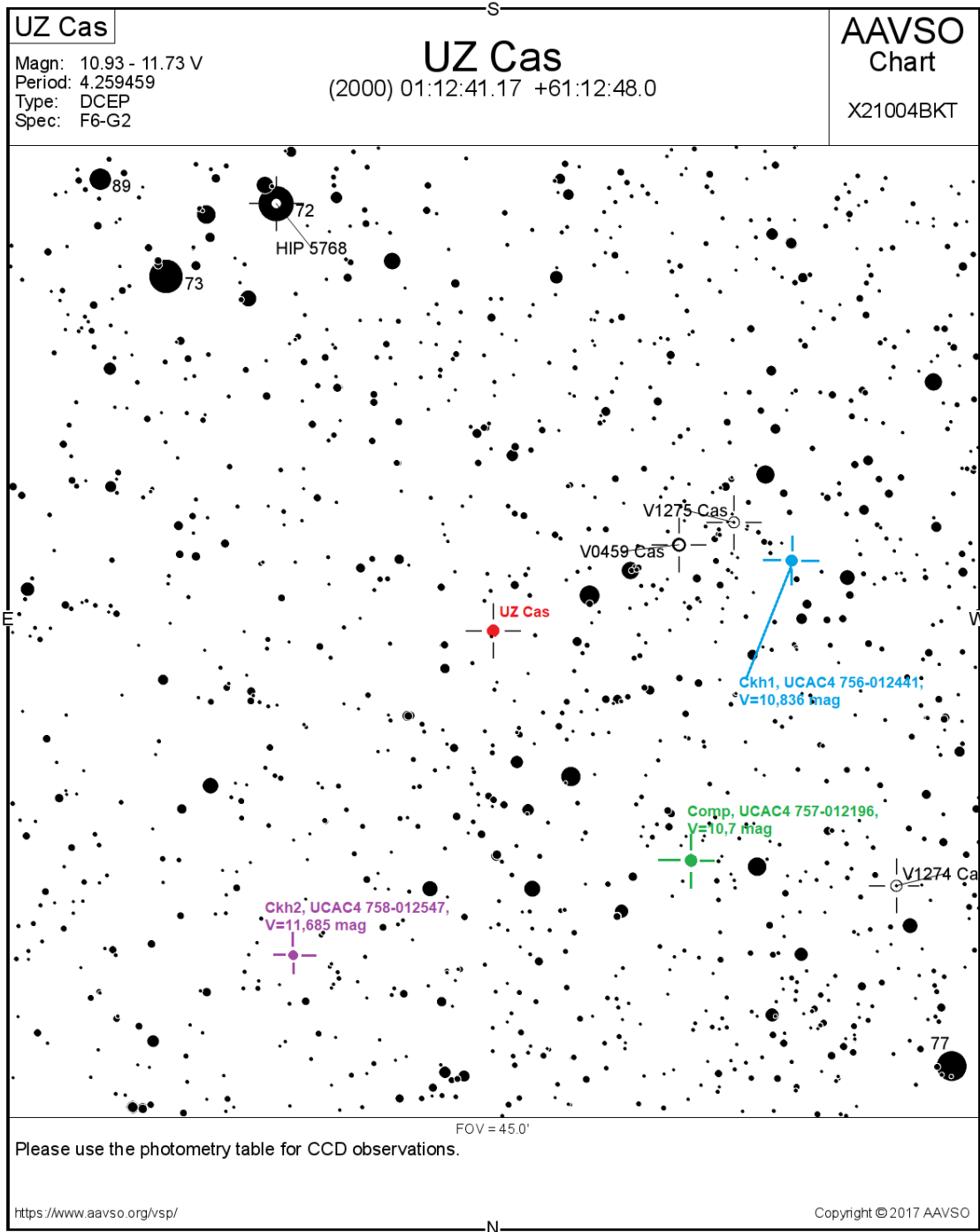Figure A1: Star chart for DF Cas.

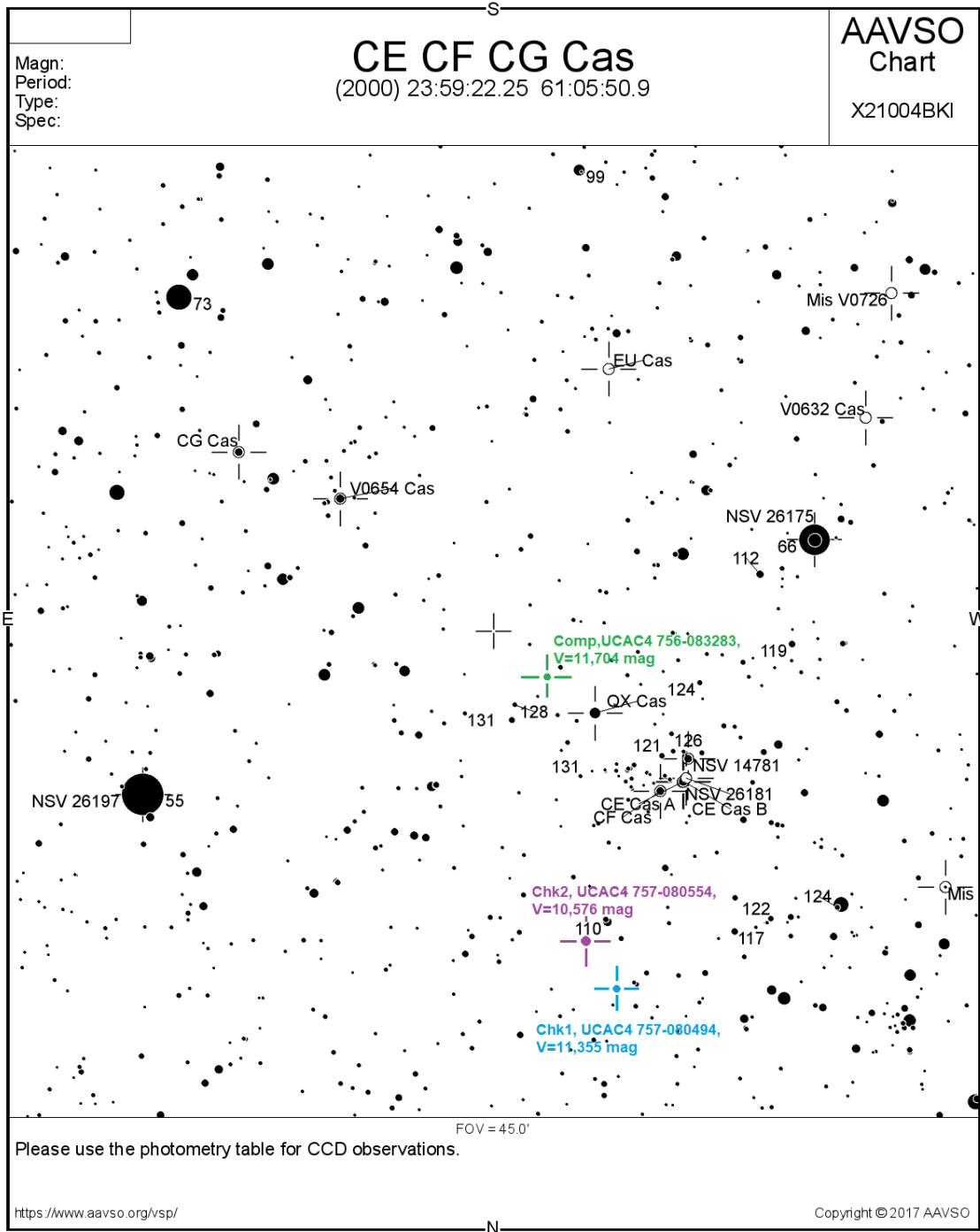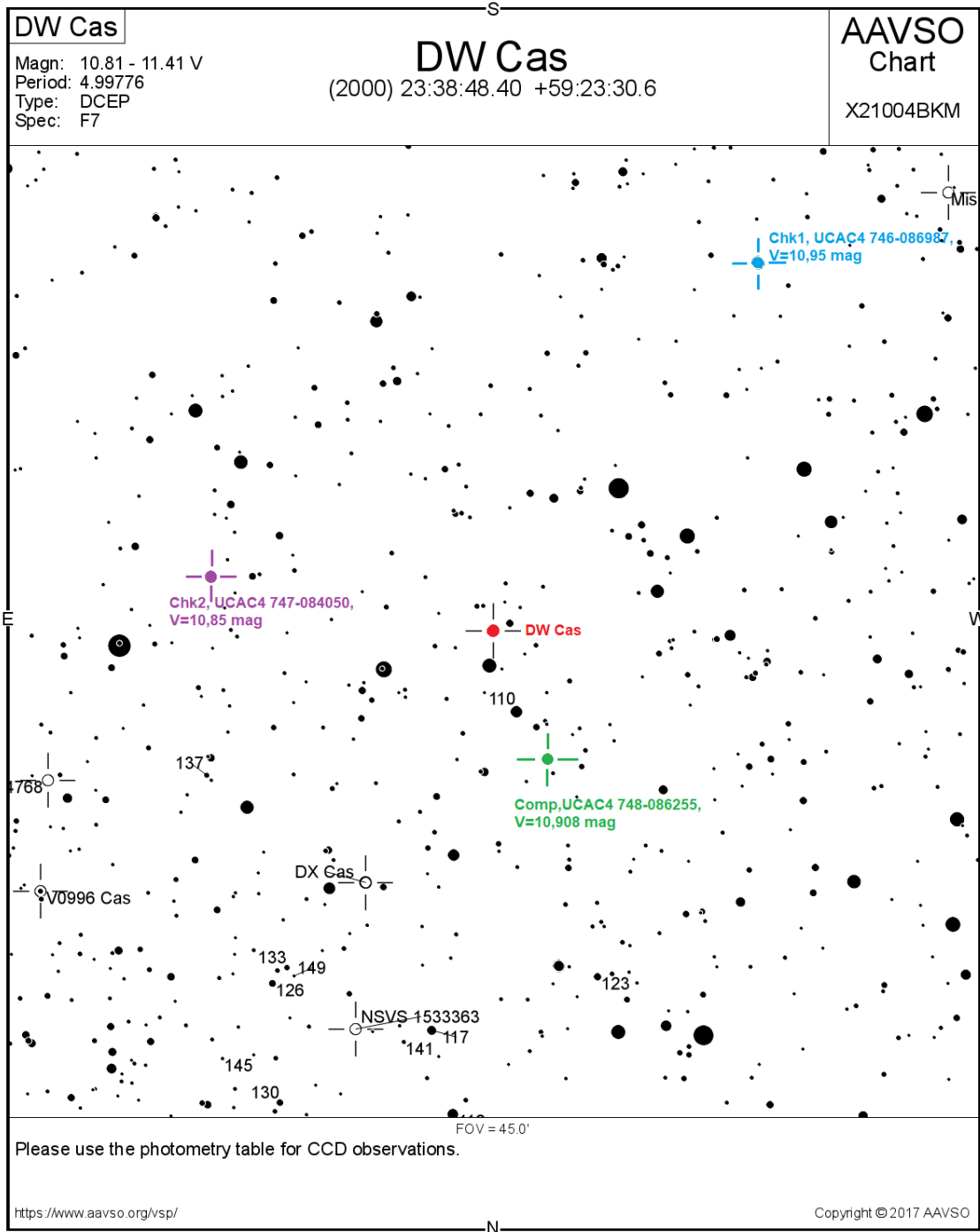Figure A2: Star chart for V395 Cas.

Figure A3: Star chart for UZ Cas.

Figure A4: Star chart for CF and CG Cas.
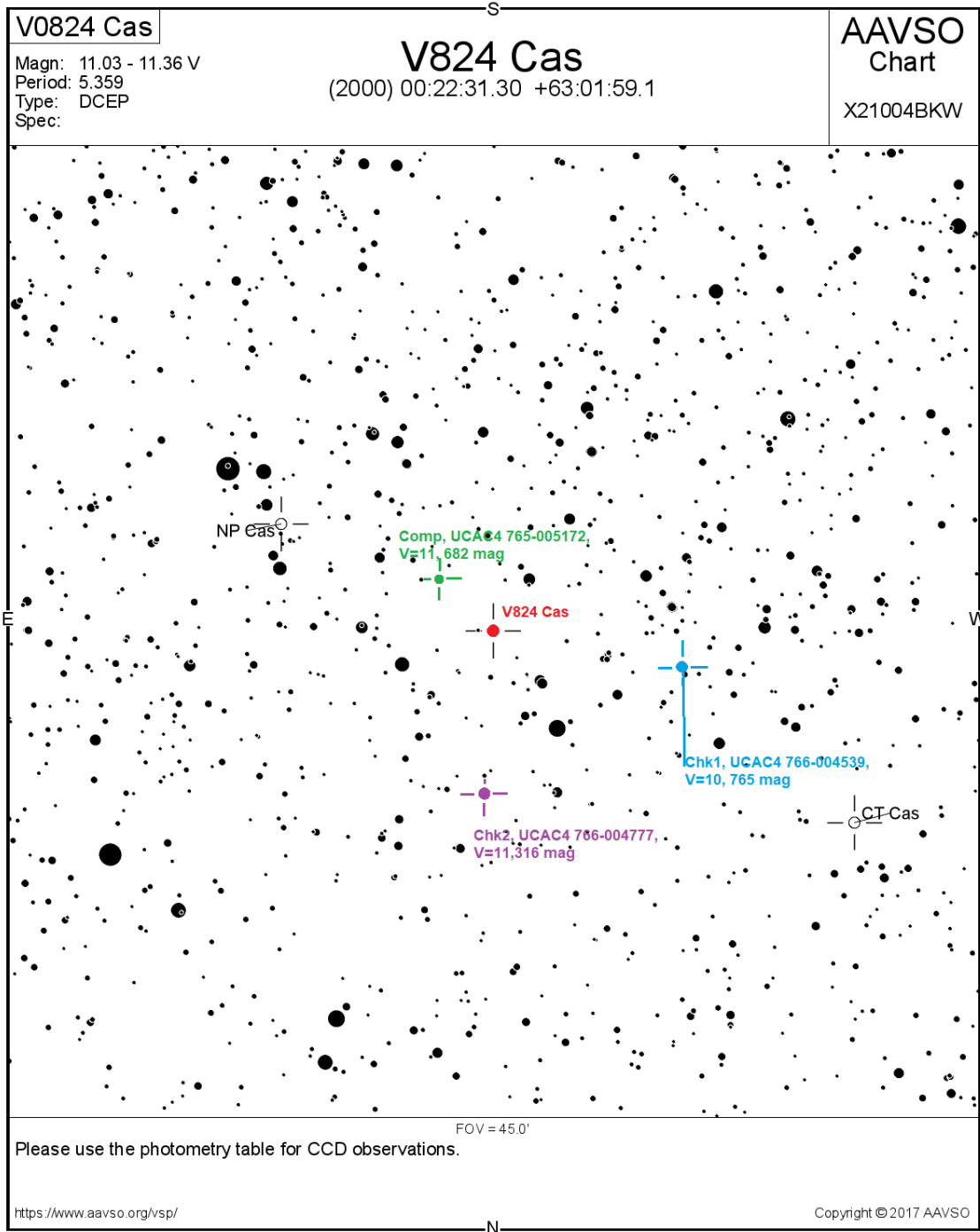
Figure A5: Star chart for DW Cas.

Figure A6: Star chart for V824 Cas.

Figure A7: Star chart for BP Cas.
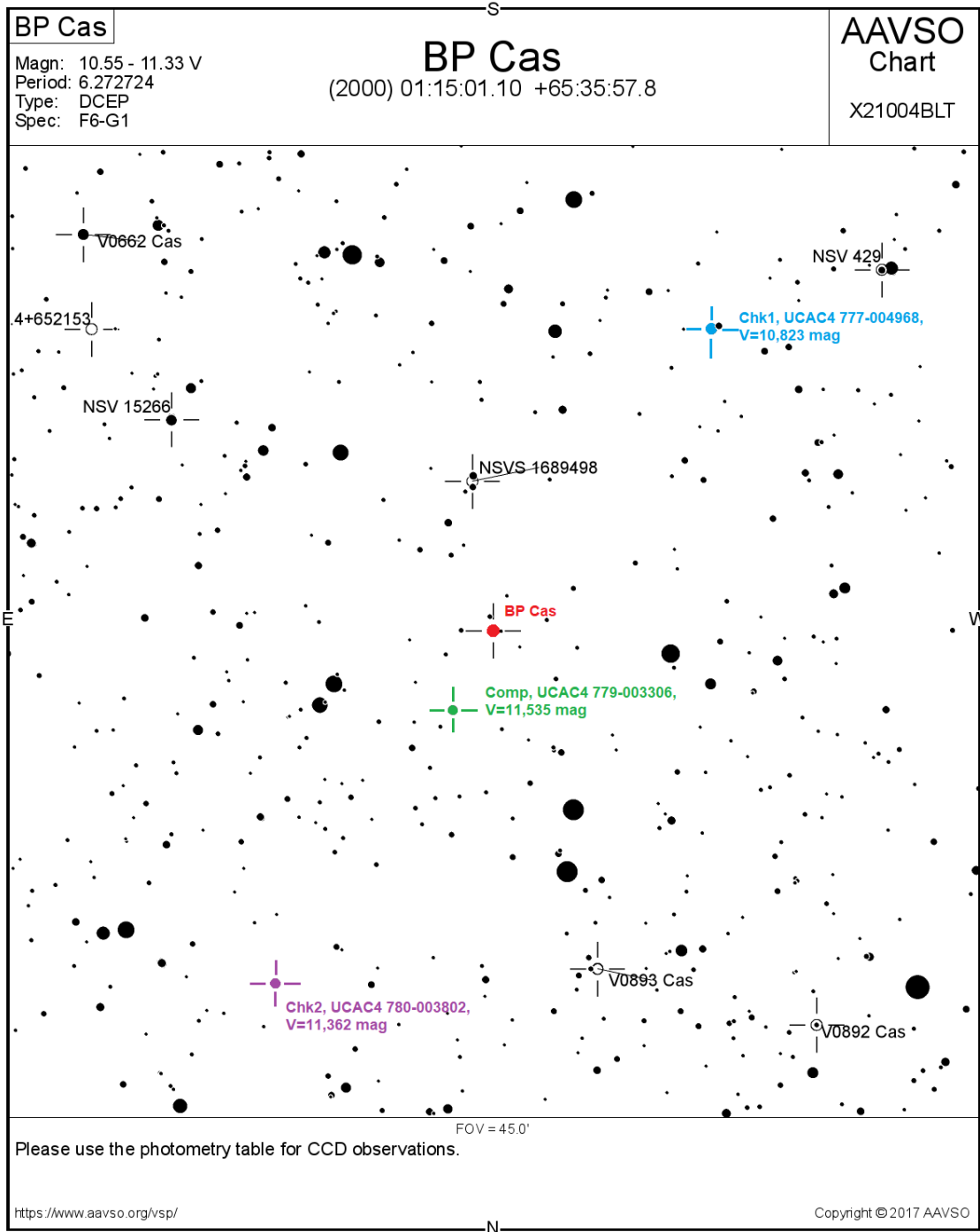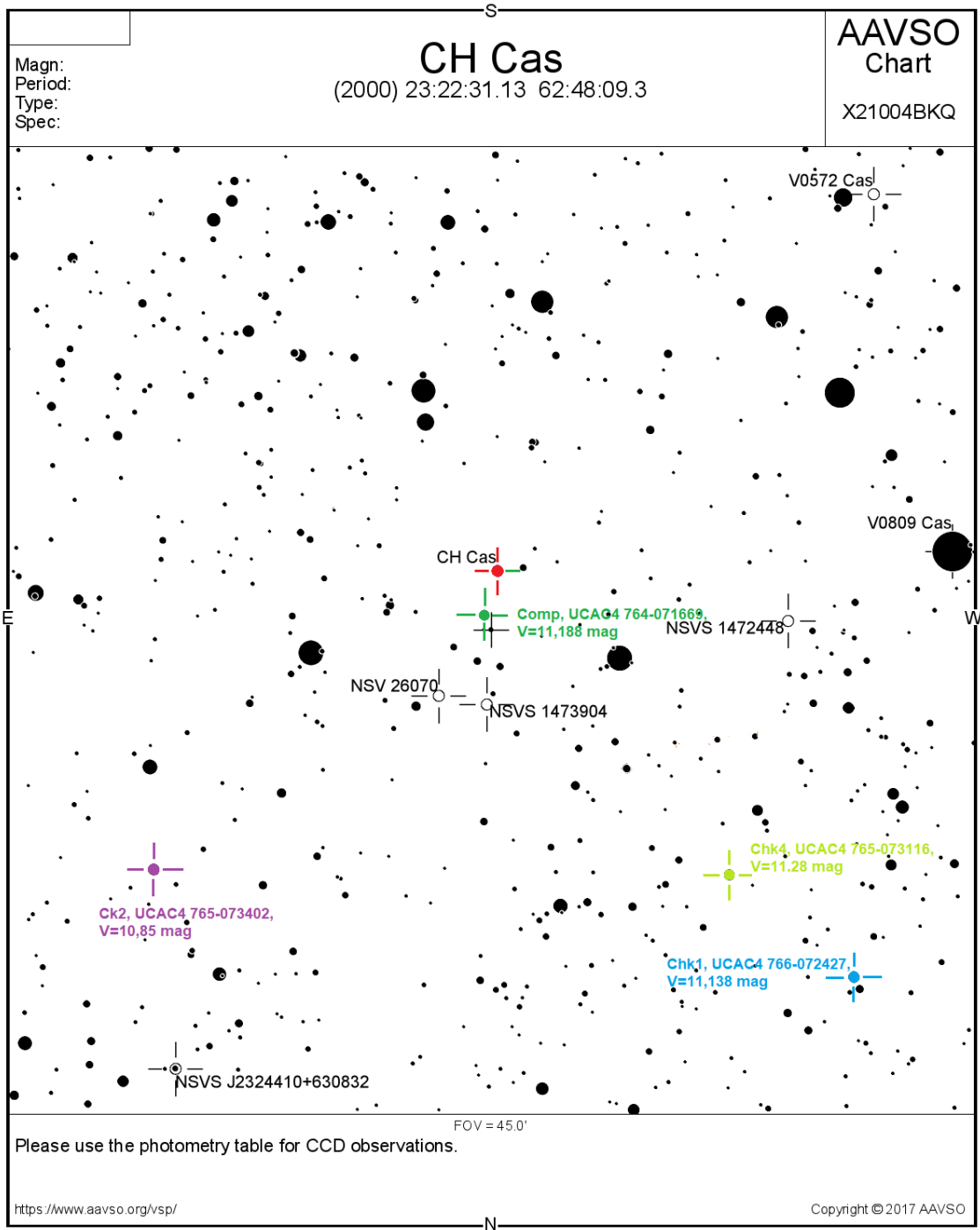
Figure A8: Star chart for CH Cas.

B Tables and images

Order of the fit	R_{21}	R_{31}	ϕ_{21}	ϕ_{31}
3	0.377	0.155	2.438	5.152
4	0.385	0.155	2.508	5.228
5	0.378	0.151	2.522	5.287
6	0.370	0.152	2.523	5.328
7	0.362	0.150	2.487	5.208
8	0.371	0.140	2.490	5.147
9	0.373	0.139	2.478	5.138

Table B1: Dependency of the Fourier coefficient on the order of the fit.

(a) ϕ_{21} coefficient.

(b) ϕ_{31} coefficient.

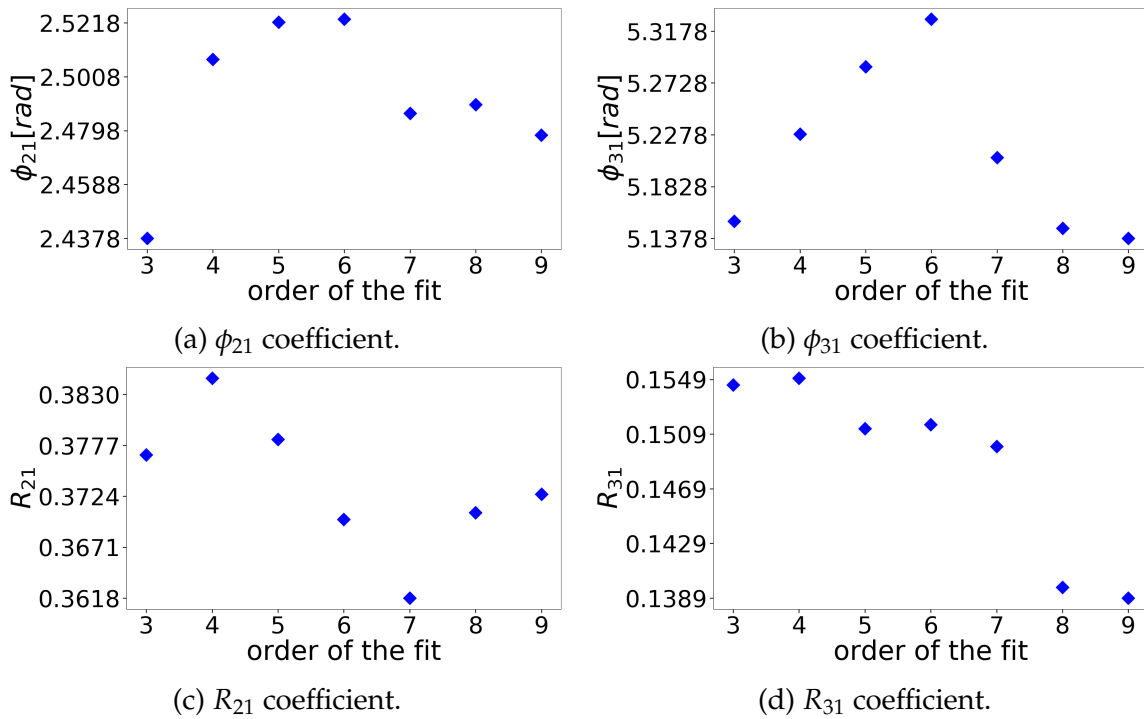(c) R_{21} coefficient.

(d) R_{31} coefficient.

Figure B1: Fourier coefficient dependency on the order of the fit for DF Cas in B filter.

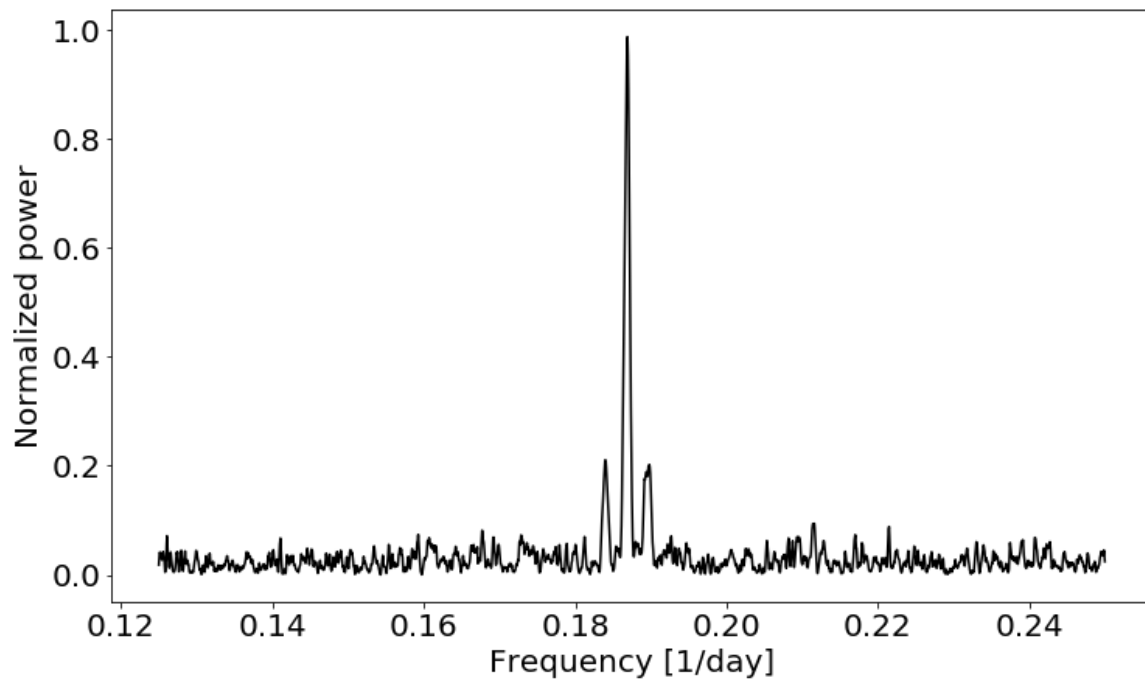| Star	Source of data
DF Cas	Antonello, Poretti, & Reduzzi (1990)
UZ Cas	Antonello, Poretti, & Reduzzi (1990)
CG Cas	Antonello, Poretti, & Reduzzi (1990)
CF Cas	Moffett & Barnes (1985)
BP Cas	Simon & Lee (1981)
CH Cas	Antonello & Morelli (1996)
V824 Cas	Berdnikov (2008)

Table B2: Data source for Fourier coefficients comparison in *V* filter.

Figure B2: Periodogram for V824 Cas.